AER/AGS Open File Report 2019-05

Alberta Energy Regulator

Three-Dimensional Property Modelling of the Paskapoo, Porcupine Hills, Scollard, and Willow Creek Formations in Southwest Alberta

AGS
ALBERTA GEOLOGICAL SURVEY

AER/AGS Open File Report 2019-05

Three-Dimensional Property Modelling of the Paskapoo, Porcupine Hills, Scollard and Willow Creek Formations in Southwest Alberta

S. Mei

Alberta Energy Regulator
Alberta Geological Survey

June 2019

ISBN 978-1-4601-3991-2

Published June 2019 by:
Alberta Energy Regulator
Alberta Geological Survey
4th Floor, Twin Atria Building
4999 – 98th Avenue
Edmonton, AB T6B 2X3
Canada

Tel: 780.638.4491
Fax: 780.422.1459
Email: AGS-Info@aer.ca
Website: www.ags.aer.ca

Contents

Acknowledgements vi
Abstract vii
1 Introduction 1
1.1 Study Area 1
2 Stratigraphic Framework and Previous Work 3
3 Data and Compilation 7
3.1 Petroleum Well Log Data 7
3.2 Water Well Data 7
4 Methods and Workflow 10
4.1 Log Analysis 10
4.1.1 Gamma Ray Log Normalization 10
4.1.1.1 Define Intervals for Gamma Ray Log Normalization 11
4.1.1.2 Through-casing Gamma Ray Log Normalization 11
4.1.2 Identify and Manage Outlier Gamma Ray Logs 11
4.1.3 Shale Volume Calculation 12
4.1.4 Density Logs Processing 12
4.1.5 Density Porosity Calculation 13
5 3D Modelling in Petrel 15
5.3 3D Property Modelling 17
5.3.1 Upscale and Transform Well Log Data 17
5.3.2 Variogram Modelling 17
5.3.3 Populate 3D Geocellular Grid 18
6 Model Quality 27
7 Observations 30
8 Summary and Discussion 32
9 References 35
Appendix – Variograms and variogram parameters 37

Tables

Table 1. Variogram parameters for the shale percentage variable in the 3D property model. 42
Table 2. Variogram parameters for the density porosity variable in the 3D property model. 42
Table 3. Variogram parameters for the water well derived shale percentage variable in the 3D property model. 42

Figures

Figure 1. Location of the study area and bedrock geology map. 2
Figure 2. Partial table of formations covering the modelled interval in this report 3
Figure 3. Cross-sections illustrating the wedge-shaped geometry of the bedrock formations overlying the Battle Formation. 4
Figure 4. Well log cross-section along line 3 in Figure 1. 9
Figure 5. Neutron-density cross plot of 1 236 well logs, filtered by gamma ray <50 API. 14
Figure 6. Well log cross-section along line 3 in Figure 1. 16
Figure 7. Isometric view of two realizations for the shale percentage model. 19

Figure 8. Isometric view of the arithmetic mean of 100 realizations (top) and the co-kriging model (bottom) for the shale percentage model. 20
Figure 9. Isometric views of the 10th (top) and 90th (bottom) percentiles for the shale percentage model. 22
Figure 10. Isometric view of the fence diagram of the kriged shale percentage model. 23
Figure 11. Isometric view of two realizations for the density porosity model. 24
Figure 12. Isometric view of the arithmetic mean of 100 realizations (top) and the co-kriging model (bottom) for the density porosity model. 25
Figure 13. Isometric view of the 10th (top) and 90th (bottom) percentiles for the density porosity model. 26
Figure 14. Isometric view of the fence diagram for the density porosity model. 27
Figure 15. Isometric view of the kriging standard deviation for the shale percentage model (top) and the density porosity model (bottom). 29
Figure 16. Cross-sections of the kriged shale percentage model. 30
Figure 17. Cross-section of the kriged shale percentage model. 31
Figure 18. Cross-sections of the kriged density porosity model. 32
Figure 19, Comparison of the shale percentage model (upper) with the sandiness model of Lyster and Andriashek (2012) (lower). 33
Figure 20. Comparison of cross-sections of geological formations and the kriged shale percentage model. The cross-section's location is shown by line 3 in Figure 1. Vertical exaggeration is 45 times. 34
Figure 21. Variogram model for the shale percentage variable in the zone for the Paskapoo and Porcupine Hills formations. 37
Figure 22. Variogram model for the shale percentage variable in the zone for the Scollard and Willow Creek formations. 38
Figure 23. Variogram model for the density porosity variable in the zone for the Paskapoo and Porcupine Hills formations. 39
Figure 24. Variogram model for the density porosity variable in the zone for the Scollard and Willow Creek formations. 40
Figure 25. Variogram model for the shale percentage variable derived from water wells for all zones. 41

Acknowledgements

The author wishes to thank Steven Lyster, Paulina Branscombe, Kelsey MacCormack and Barry Fildes for technical and editorial reviews that have considerably improved the manuscript. The author also thanks Mike Berhane for beneficial discussions on log analysis, and Laurence Jayawardane for assistance with the modelling software.

Abstract

A three-dimensional (3D) property model of sandiness/shaliness and porosity was developed for the uppermost Cretaceous–Paleogene bedrock deposits in southwest Alberta. The bedrock units are the Scollard Formation and its equivalent Willow Creek Formation, and the younger Paskapoo Formation and its equivalent Porcupine Hills Formation. These units represent a shale/mudstone-siltstone-sandstone sequence of high energy alluvial and fluvial floodplain sedimentation. The percentage of shale is inversely related to the sandstone abundance in the sequence and was calculated from a combination of GR logs from oil/gas wells and lithological descriptions from water wells. The porosity was calculated from bulk density logs from oil/gas wells. The 3D property model covers an area over 91 000 km^2 and represents an eastward-thinning wedge, with a present-day maximum thickness of over 1000 m close to the Foothills of the Canadian Rocky Mountains, that pinches out towards the plains. The model was created in Schlumberger's Petrel 2015 and is appropriate for regional-scale (1:100 000) assessments rather than site-specific investigations. Several trends emerge from the 3D modelling, including:

- A basal sandstone unit within the Paskapoo Formation is well developed in the central part of the study area. This unit becomes discontinuous and absent in the northern and southern parts of the study area.
- Above the basal sandstone unit is a mudstone-dominated interval in the middle part of the Paskapoo Formation. It grades into an interval of higher sandstone abundance towards the west-central section of the 3D model. The mudstone interval grades into an interval of higher sandstone abundance in the upper portion of the Paskapoo Formation.
- The Porcupine Hills Formation in the southwest of the 3D model does not show a three-layer structure, but is characterized by a sandier interval in the lower part and a mudstone and siltstone interval in the middle and upper part of the formation.
- The porosity generally increases up-dip from west to east for both the Scollard Formation and the Paskapoo/Porcupine Hills formations, and is generally greater in the northern part than in the southern part of the study area.

The 3D model offers insight into the regional distribution of highly porous sandstone within near-surface bedrock deposits. It can be used to conceptualize the hydrostratigraphy, assuming that sandstone abundance can be used as a proxy for permeability.

1 Introduction

The Paskapoo and equivalent Porcupine Hills formations collectively are one of the largest and most intensely used bedrock aquifer systems in Alberta. They include a heterogeneous assemblage of nonmarine mudstone and siltstone together with single- and multi-storey sandstone units that are not easily classified within a hydrostratigraphic framework. A major component of the hydrogeological characterization was the development of a regional hydrostratigraphic model to identify subsurface zones of similar lithology and/or porosity. The spatial distribution of heterogeneous porous sedimentary rocks is regarded as one of the most important elements in the construction of a regional groundwater-flow model (Fogg, 1986).

The objective of this project was to evaluate the ability to employ well log data from the petroleum industry and water well data as the first step toward an assessment of the spatial characteristics of the sandiness and porosity of the Paskapoo and Porcupine Hills formations. The underlying Scollard Formation and equivalent Willow Creek Formation were also included. A 3D model was created where the bedrock is represented by the percentage of shale and porosity, determined from a combination of oil- and gas-well gamma ray (GR) and bulk density logs and lithological descriptions from water wells. The 3D renderings of the subsurface bedrock enhance the conceptualization of hydrostratigraphy at a scale appropriate for regional assessments rather than site-specific investigations. This report presents the results and methodology used to model the properties of the Paskapoo and Porcupine Hills formations and the underlying Scollard and Willow Creek formations in southwest Alberta.

1.1 Study Area

The study area is over 91 000 km^2 and located in southwest Alberta (Figure 1). We used the extent of the base of the Scollard/Willow Creek formations from version one of the 3D Provincial Geological Framework (PGF) (Branscombe et al., 2018) as the study area for the project. This ensures that the extent not only covers the entire area of the Paskapoo and Porcupine Hills formations, but also includes a buffer zone beyond the limit of the Paskapoo and Porcupine Hills formations to eliminate any potential edge effects in 3D modelling. As a result, the bedrock units modelled include the near-surface Paskapoo/Porcupine Hills formations and the underlying Scollard/Willow Creek formations (Figure 2). The northeast boundary of the study area is close to the erosional edge of the Scollard/Willow Creek formations. To the west it is defined by the Cordilleran deformation belt. Figure 1 shows a map of the study area boundary.

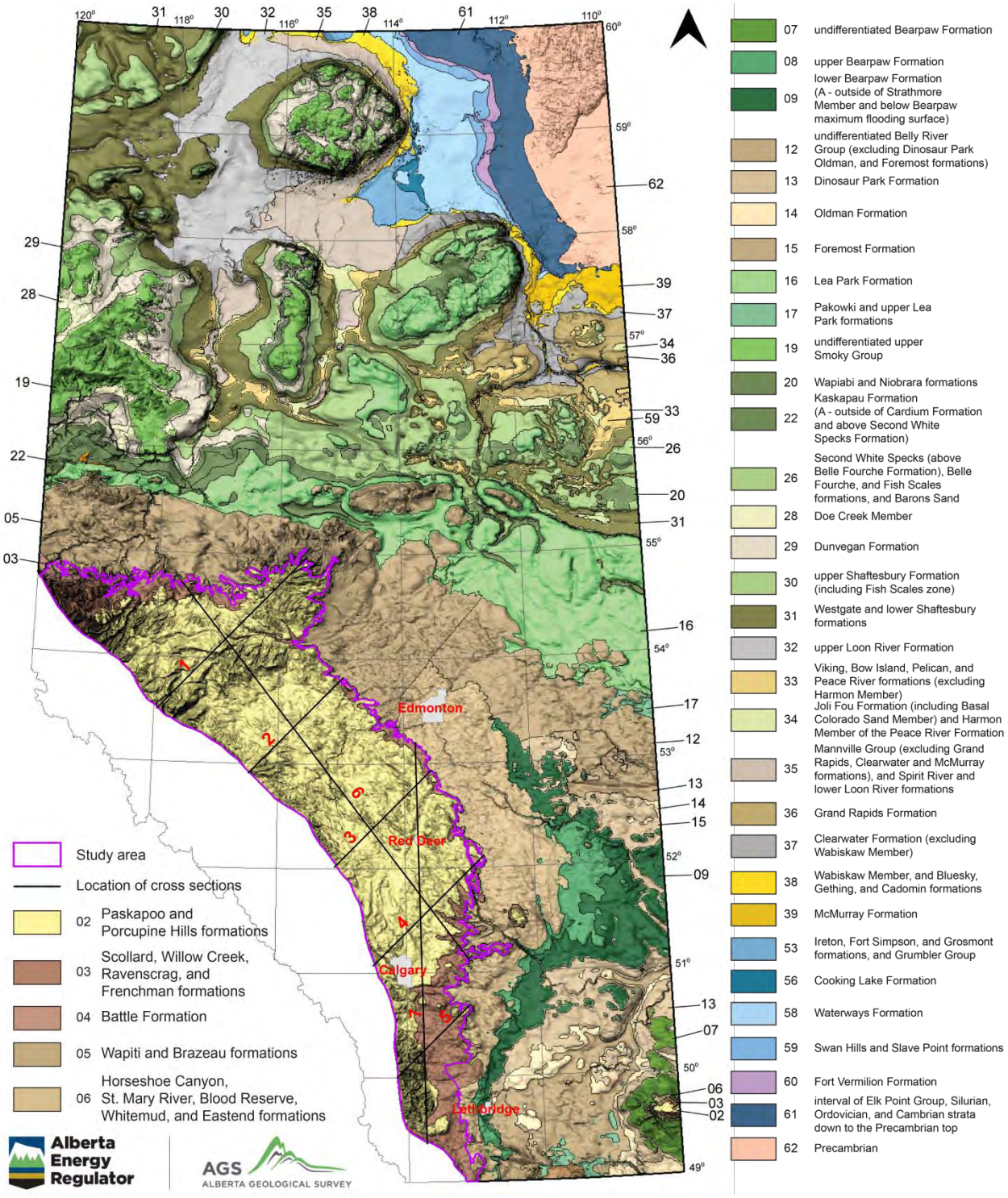

Figure 1. Location of the study area and bedrock geology map (modified from Alberta Geological Survey, 2019). Cross-section lines (labelled in red) are referenced in subsequent figures.

2 Stratigraphic Framework and Previous Work

The Paskapoo and Porcupine Hills formations are Paleocene in age and represent the youngest preserved bedrock deposits in the area of their occurrences (Demchuk and Hills, 1991; Lerbekmo et al., 1992; Hamblin 2004; Chen et al., 2007; Grasby et al., 2008; Lerbekmo and Sweet, 2008; Prior et al., 2013). The Paskapoo, Porcupine Hills and the underlying Scollard and Willow Creek formations represent a sequence of high energy alluvial and fluvial floodplain sedimentation associated with the Laramide Orogeny and the final stage of the foreland evolution in the Western Canada Sedimentary Basin (WCSB) (Hamblin, 2004). Figure 2 shows a table of formations covering the relevant strata (after Alberta Geological Survey, 2015). The bedrock preserved at present represent an erosional remnant of an originally much thicker and more extensive clastic wedge deposited in the subsiding foreland basin, developed between the deforming mountain front and the adjacent craton, in response to thrust loading of the Rocky Mountains to the west. They form a vast eastward-thinning wedge, with a present-day maximum thickness of over 1000 m in the foothills of the Canadian Rocky Mountains, that pinches out towards the plains (Grasby et al., 2008; Hamblin 2004). Figure 3 shows two cross-sections illustrating the wedge-shaped geometry of the Paskapoo/Porcupine Hills and the underlying Scollard/Willow Creek formations.

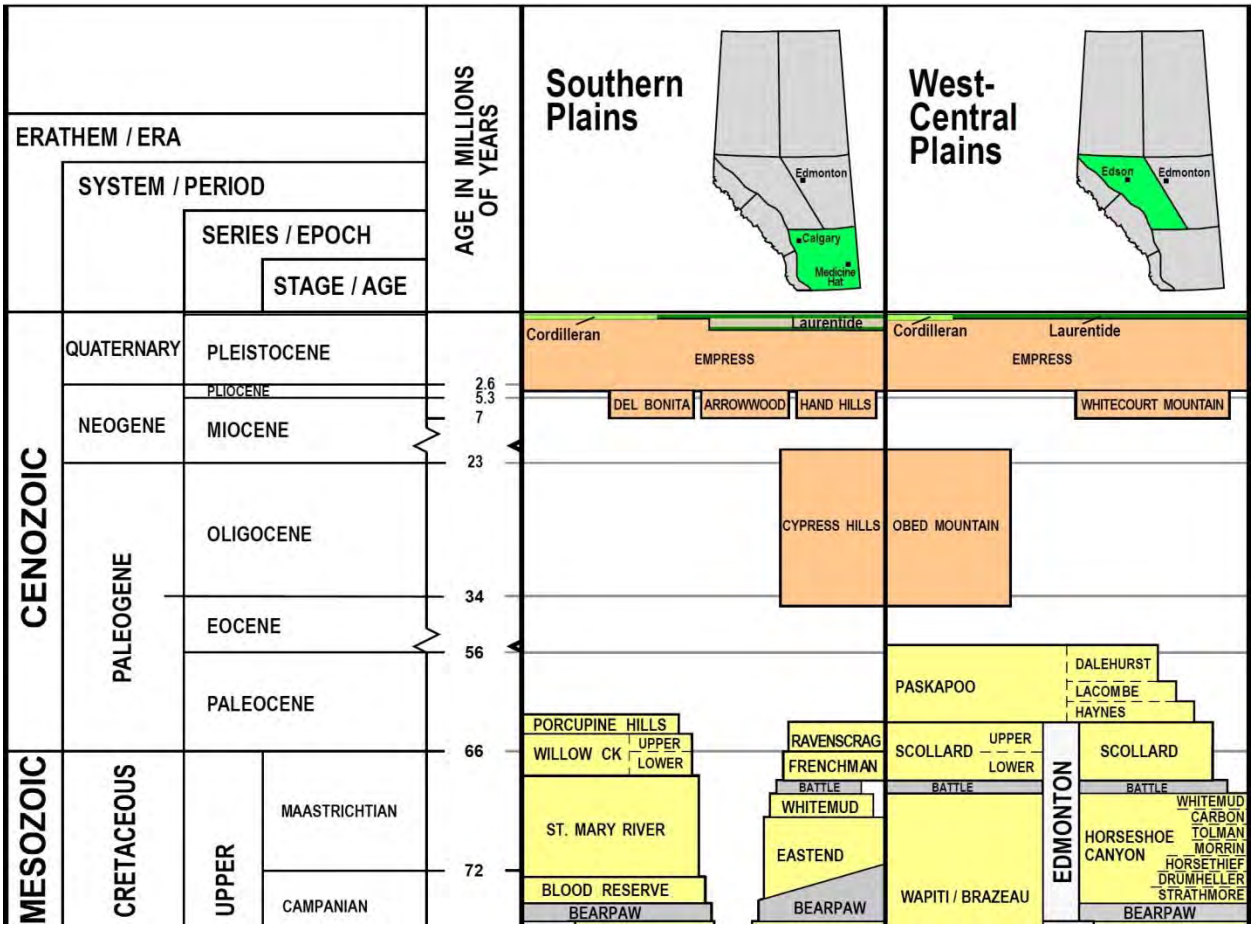

Figure 2. Partial table of formations covering the modelled interval in this report (modified from Alberta Geological Survey, 2015)

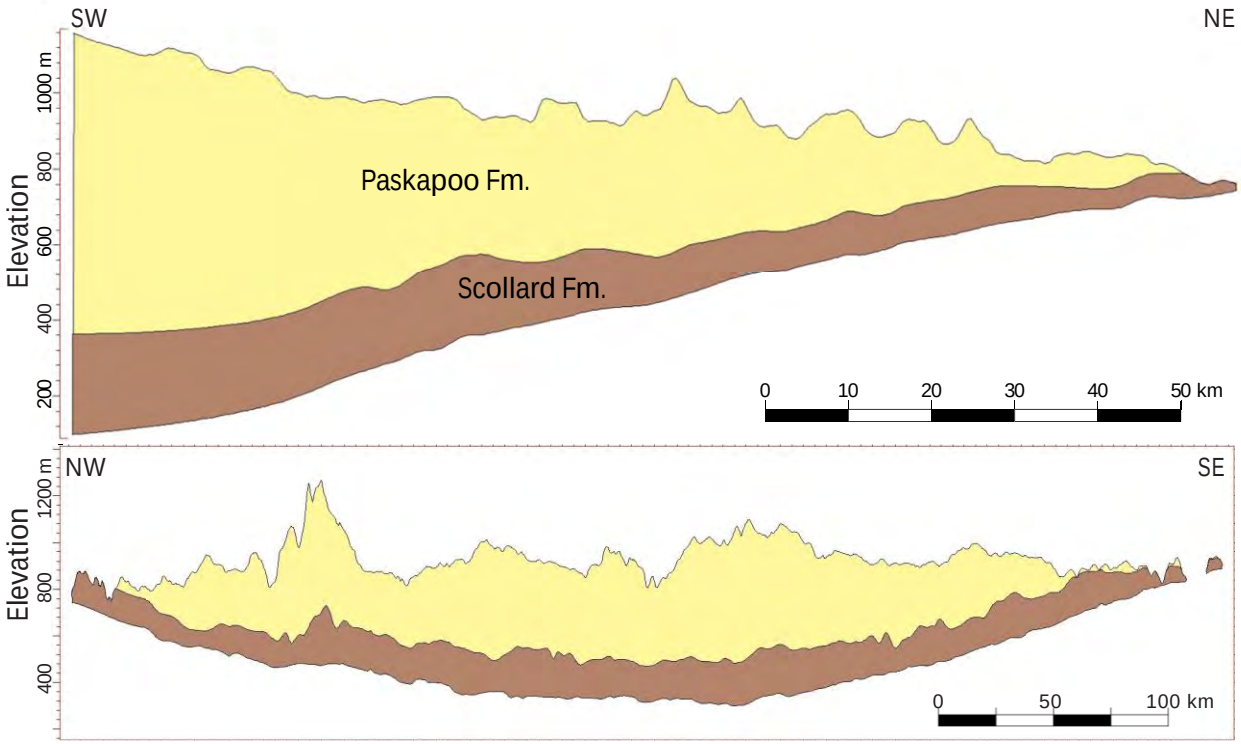

Figure 3. Cross-sections illustrating the wedge-shaped geometry of the bedrock formations overlying the Battle Formation. Locations of the two cross-sections are indicated by line 3 and line 6, respectively, in Figure 1. Vertical exaggeration is 45 times (upper) and 100 times (lower).

The Porcupine Hills Formation was generally believed to be the equivalent of the Paskapoo Formation and Jerzykiewicz (1997) suggested that the Porcupine Hills is simply an arid-climate facies of the Paskapoo Formation. However, Lerbekmo and Sweet (2000) suggested that the lowest part of the Porcupine Hills Formation correlates to the upper Scollard Formation and the rest is equivalent to the Paskapoo Formation, based on the study of magneto- and biostratigraphy in the Calgary area. They also indicated that between the two members of Porcupine Hills Formation is a significant hiatus that is equivalent to the erosional surface at the base of the Paskapoo Formation in the Red Deer River valley. These correlations may be evident at the studied outcrops, or a local scale; however, regional correlations have largely remained conceptual in nature and difficult to apply. In this report, the Paskapoo and Porcupine Hills formations are mapped as one lithological continuum.

The placement of the lower boundary of both the Paskapoo Formation (Demchuk and Hills, 1991; Jerzykiewicz, 1997; Hamblin, 2004) and the Porcupine Hills Formation (Williams and Dyer, 1930; Braman and Sweet, 1990; Jerzykiewicz, 1997) has been under debate. Regardless, it is generally accepted that the first thick sandstone that overlies the uppermost coal seam of the Ardley coal zone of the Scollard Formation defines the base of the Paskapoo Formation (Gibson, 1977; Demchuk and Hills, 1991). The base of the Paskapoo Formation was also shown as a basin-wide, erosional unconformity cutting into the underlying Scollard Formation (Jerzykiewicz, 1997; Lerbekmo and Sweet, 2008; Burns et al., 2010).

To the southwest, the base of the Porcupine Hills Formation is more difficult to define because criteria such as coal beds and distinct log responses are lacking (Jerzykiewicz, 1997; Lerbekmo and Sweet, 2000). It has been suggested that the Porcupine Hills Formation disconformably overlies a paleosol horizon atop the Willow Creek Formation (Braman and Sweet, 1990; Jerzykiewicz, 1997). The upper boundary of the Paskapoo and Porcupine Hills formations is an erosion surface that marks the bedrock top across their extent (Parks and Andriashek, 2009). Nurkowski (1985) indicated that coal beds in the near-surface of the

Alberta Plains had previously been buried by sedimentary cover at depths of at least 900 m, implying that the thickness of the Paskapoo and Porcupine Hills formations may have been significantly greater prior to erosion. The erosional surface is unconformably overlain by discontinuous deposits of upper Neogene gravel or Quaternary sediment at the ground surface (Figure 3).

Attempts have been made to subdivide the Paskapoo Formation based on the occurrence and distribution of sandstone, mudstone/siltstone, and coal (Demchuk and Hills, 1991), the presence of a disconformable sandstone/conglomerate unit within the formation (Jerzykiewicz, 1997), and palynomorph, mammal biostratigraphy and magnetostratigraphy (Lerbekmo and Sweet, 2000, 2008; Lerbekmo et al., 2008). Although these subdivisions may be evident at the studied borehole and outcrop at a local scale, their regional correlations have largely been conceptual in nature and difficult to apply.

Demchuk and Hills (1991) first subdivided the Paskapoo Formation into three members, based on outcrop observations, core descriptions from boreholes and palynomorph biostratigraphy. The lowermost Haynes Member is dominated by thick, massive, coarse-grained channel sandstones that form a regionally extensive and apparently continuous unit up to 100 m thick (Demchuk and Hills, 1991; Hamblin, 2004; Grasby et al., 2008). The Paskapoo Formation is commonly referred to as "the Paskapoo Sandstone" owing to the fact that outcrops of the formation are often biased towards these massive, cliff-forming channel sandstones of the Haynes Member. The sandstone of the Haynes Member is also recognizable in subsurface by its uniform, blocky signature and abrupt lower contact with siltstone and mudstone of the underlying Scollard Formation in GR and resistivity logs.

Whereas channel sandstone bodies of the Haynes Member are prominent in outcrop, the overlying Lacombe Member is the dominant component of the Paskapoo Formation and characterized by overbank interbedded siltstone, mudstone, shale, and coal with minor fine- to medium-grained channel and splay sandstones (Demchuk and Hills 1991). It is rarely exposed in outcrop due to its recessive nature, but is inferred to form the present-day bedrock surface over much of the central subcrop area of the Paskapoo Formation (Grasby et al., 2008).

The uppermost Dalehurst Member of the Paskapoo Formation, as defined by Demchuk and Hills (1991), consists of interbedded sandstone, siltstone, mudstone, and shale with at least five thick (1.3– 6.1 m) coal seams. The Dalehurst Member is differentiated primarily by the occurrence of thick coal beds of the Obed-Marsh coal zone and only preserved as an erosional remnant in the Hinton area (Demchuk and Hills 1991; Hamblin, 2004). This member cannot be easily correlated eastward into the plains, although Demchuk and Hills (1991) debated whether these thick coal beds were lateral facies equivalents of thinner coal seams in the upper part of the Lacombe Member to the southeast in the Red Deer area.

In contrast to the three-member subdivisions of Demchuk and Hills (1991), Jerzykiewicz (1997) divided the Paskapoo Formation into informal upper and lower members. A thick, continuous, basin-wide sandstone unit that correlates to the basal sandstone unit of Demchuk and Hills (1991), the Haynes Member is attributed to flash-flood deposition and defines the base of the lower member. Jerzykiewicz (1997) suggested that the base of the upper member is marked by the High Divide Ridge conglomerate to the north, and by escarpment-forming thick sandstone to the south.

No attempt has been made to subdivide the Paskapoo-equivalent portion of the Porcupine Hills Formation as defined by Lerbekmo and Sweet (2000). The stratigraphic subdivisions of the Paskapoo Formation by Demchuk and Hills (1991) and Jerzykiewicz (1997) were mainly based on observations at point locations rather than on regional correlation and mapping of rock properties from large datasets. Neither study generated interpretations of the distribution and boundaries of rock properties of the members in the subsurface.

While it is difficult to define regional stratigraphic relationships within the Paskapoo Formation using conventional geological mapping methods, several studies for groundwater aquifers have applied

automated analytical mapping methods to digital log datasets to map the spatial variation of rock properties within the Paskapoo Formation. Chen et al. (2007) calculated net sandstone thickness from quantitative analysis of GR logs, and porosity from sonic and density logs in wells completed within the lower part of the Paskapoo Formation. Grasby et al. (2008) incorporated water well litholog data to address the gap in GR coverage in Chen et al. (2007) caused by cased portions of oil and gas wells in the uppermost part of the Paskapoo Formation. Both Chen et al. (2007) and Grasby et al. (2008) identified a northwest trend of high sandstone ratio within the Paskapoo Formation, parallel to the deformation belt and the axis of the Alberta Basin.

Parks and Andriashek (2009) mapped the spatial variability of sandstone abundance from the analysis of GR logs in 50 m thick slices through the Scollard and Paskapoo formations. The depth-slice analysis recognized three intervals within the Paskapoo Formation. The lowermost 150 to 200 m of the Paskapoo Formation includes regionally extensive zones of >40% sandstone abundance, forming an elongated trend subparallel to the Cordilleran deformation front. This lower, sandy interval is capped by >300 m of sedimentary rock with generally <40% vertically averaged sandstone abundance. On top of this muddy interval, a narrow belt of high sandstone abundance was mapped adjacent to the Cordilleran deformation front. These three intervals were considered to be roughly correlative to the three members outlined by Demchuk and Hills (1991).

Building on the work of Parks and Andriashek (2009), Lyster and Andriashek (2012) also used a depth-slice analysis method that incorporated water well lithology data. They applied a 25m-thick slicing and employed a probabilistic approach, using geostatistical methods to model the proportion of sandstone within specified volumes within the Paskapoo Formation. Following the same procedures described by Parks and Andriashek (2009), for each GR log:

1. intervals with a GR value ≤75 API were assigned to sandstone;
2. the thickness of every interval with a GR value ≤75 API was summed;
3. the summed total was expressed as a percentage of sandstone for each 25 m thick slice; and
4. a geostatistical modelling algorithm was applied to the values of sandstone percentage to construct a 3D model by estimating values of sandiness at unsampled locations for each voxel in the 3D model.

The 3D model enabled the examination of the regional distribution trend of sandiness within the Paskapoo Formation. Similar to Parks and Andriashek (2009), Lyster and Andriashek (2012) recognized three regional sandstone/mudstone trends from the series of stacked slice in the 3D model; they include a lower, up to 125 m thick interval, dominated by sandstone, a middle, 225 to 250 m thick interval, dominated by mudstone and siltstone, and an upper, 300 to 400 m thick interval, of high sandstone percentage. These three intervals were named, in ascending order, the Haynes aquifer, the Lacombe aquitard and the Sunchild aquifer, and related to the three members of Demchuk and Hills (1991) respectively, even though no direct correlation was implied (Lyster and Andriashek, 2012).

The 3D model of sandiness also enabled the approximation of boundary surfaces of the aquifers by querying the model to identify the cells that meet different isovalue cutoffs. Lyster and Andriashek (2012) defined the upper surface of the Haynes aquifer to be the top of the sandstone body where the sandstone abundance in a 25 m thick cell is 55% or greater, and that of the Lacombe aquitard to be the top of the non-sandy material (siltstone and/or mudstone) in the model where the sandstone abundance in a 25 m thick cell is less than 35%.

As mentioned previously, the Paskapoo and Porcupine Hills formations are the uppermost bedrock units across their subcrop extent; consequently, steel casing was used to generally protect the upper parts of the formation from drilling fluids when a well was drilled. In many locations, this casing depth extends as much as 150 m below surface. GR logs from most oil and gas wells drilled prior to 2006 did not extend to surface, but terminated at the base of the cased portion of the hole. As of November 1, 2006, new

regulations were instituted that require operators to record the natural GR response of subsurface units to the ground surface (EUB, 2006). As a result, there has been a large influx of through-casing GR logs covering the near-surface portion of the Paskapoo Formation. While the through-casing GR logs were excluded from analysis in the studies mentioned previously, Quartero et al. (2015) took advantage of the new regulation and included through-casing GR logs from over 1000 wells drilled post-2006 in their study. Before using the through-casing GR logs, Quartero et al. (2015) corrected the bias caused by suppression of the GR signature by the surface casing. They normalized the through-casing GR logs across the study area by employing a statistical normalization procedure using constants derived from analogous strata in uncased portions of the Paskapoo Formation and the Scollard Formation (Quartero et al., 2014).

Quartero et al. (2015) applied the same depth-slice mapping method as used in Parks and Andriashek (2009) and Lyster and Andriashek's (2012) studies to derive the sandstone net-to-gross maps, except they sliced the Paskapoo Formation into two equal-thickness intervals for capturing regional trends and three equal-thickness intervals to focus more detailed analysis on the northern portion of the study area with a greater well density. Like the previous studies, Quartero et al. (2015) recognized three intervals that are respectively correlative to the three members of Demchuk and Hills (1991). In addition, Quartero et al. (2015) suggested that the basal Haynes sandstone unit is restricted to the southern portion of the Paskapoo Formation and the middle Lacombe Member directly overlies the Scollard Formation in the northern portion of the Paskapoo Formation where the Haynes Member is absent. Quartero et al. (2015) also recognized a 5 000 km^2 feature with high net-to-gross values in the upper portion of the Paskapoo Formation in the northern part of their study area, and interpreted this feature as a Paleocene distributive fluvial system or the result of fixed-outlet channel belt avulsion.

3 Data and Compilation

3.1 Petroleum Well Log Data

In total, over 154 000 petroleum wells were included in the Petra project for this study. In addition, over 200 AGS boreholes were also added to the project. A bare earth LiDAR DEM was used to check the surface locations of the petroleum wells. Those wells with an elevation difference between the KB and LiDAR DEM greater than 50 m were excluded from analysis. Of the remaining wells, 35 945 had a GR and/or bulk density log that covered the interval from 50 m below the base of the Scollard Formation to the bedrock surface; these wells were used for further analysis.

3.2 Water Well Data

The water well data used in this study include drillers' descriptions of geological material or lithology. The quality of these descriptions is dependent on the driller's ability to recognize lithological changes from drill cuttings, interpret the behaviour of the drilling rig in response to different rock types, and be knowledgeable about the local geological setting. Water well lithologs may not have sufficient quality to be used in a meaningful interpretation of geology; however, Lyster and Andriashek (2012) indicated that water well lithologs provide sufficient quality information suitable for characterizing sandiness at a regional scale. Water wells generally do not penetrate to depths >150 m, and this results in little spatial overlap with the petroleum GR log data for the near surface interval of the bedrock (Figure 4). The water well logs are numerous and provide useful information on lithology from the surface down to the first source of potable water (generally to depths of <150 m). Thus, they better represent the geology of the uppermost parts of the Paskapoo, Porcupine Hills and Scollard formations (Figure 4).

Slattery et al. (2011) translated more than 2 700 unique water well drillers' descriptions of geological material into 25 lithology terms, including 9 terms for bedrock materials. The 9 bedrock terms were

further collapsed into a trimodal classification in this study: sandstone, siltstone, and shale. An indicator value (Johnson and Dreiss, 1989) of 0 (0% shale) was assigned for every described interval in a water well litholog if the lithology was recorded as sandstone, a value of 0.5 (50% shale) was assigned if the lithology was recorded as siltstone, and a value of 1 (100% shale) was assigned if the lithology was recorded as shale, mudstone, claystone, coal, or other low permeability rocks. This arbitrary assignment was intended to identify the distribution trend of high, medium, and low porosity rock units and the particular shale percentage value is not of direct interest.

The coded water well data were converted to shale percentage logs in Petra and then imported into Petrel. Unlike Lyster and Andriashek's (2012) report, where the coded water well data and the GR derived data were combined and averaged into a single dataset for the 3D modelling, in this study the coded water well data were treated as a separate variable and used as a secondary variable in modelling the shale percentage for the Scollard/Willow Creek and the Paskapoo/ Porcupine Hills formations, with the shale percentage derived from the GR logs being the primary variable.

In total, 86 184 water wells were found in the study area and used for this project.

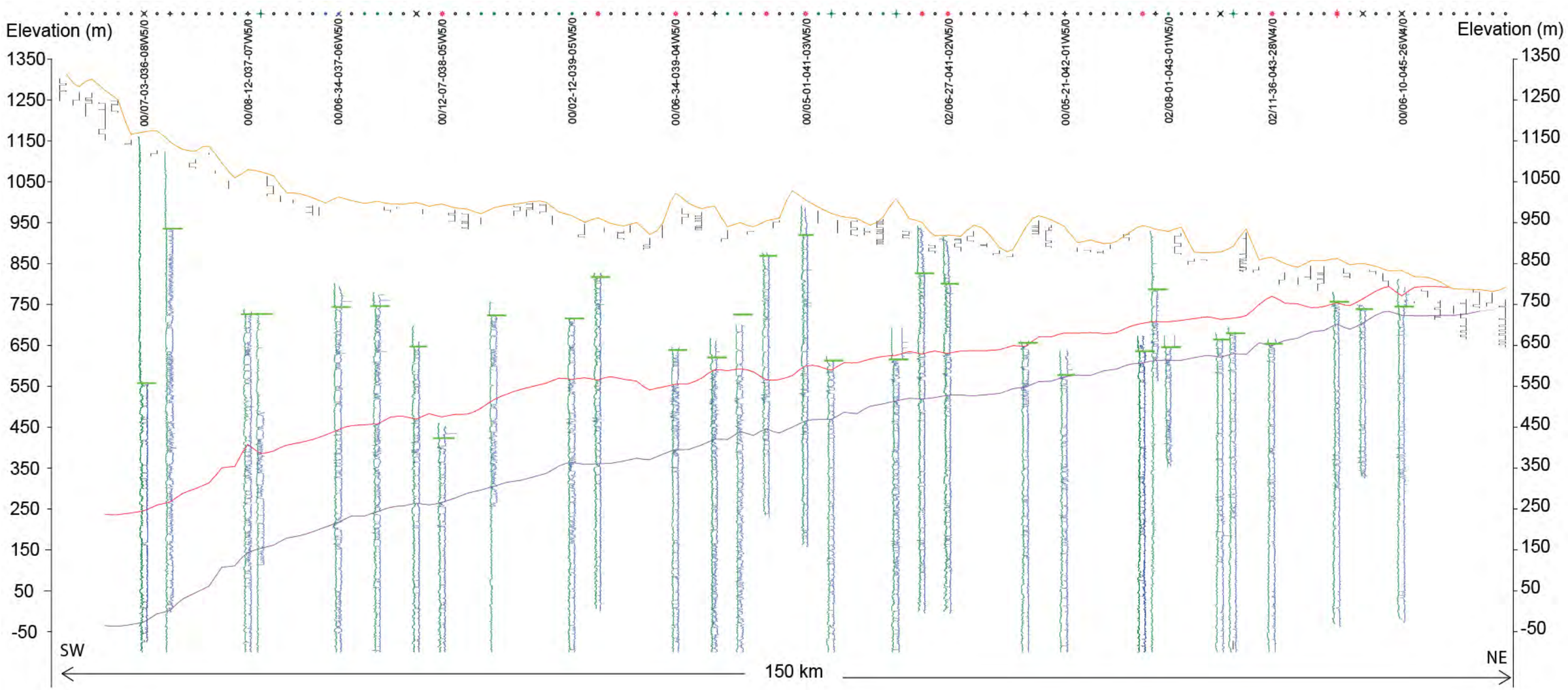

Figure 4. Well log cross-section along line 3 in Figure 1. Logs: black is the coded shale percentage log from water wells; dark green is the GR log from oil/gas wells; blue is the bulk density log. Horizons: orange is KB; red is the base of the Paskapoo Formation; purple is the base of the Scollard Formation; horizontal green bars indicate the base of surface casing. Top row are oil/gas well and water well symbols, and only selected oil/gas wells are labelled.

4 Methods and Workflow

This section outlines the workflow for 3D property modelling using petroleum geophysical logs and water well lithological data. This workflow includes steps from log analysis in Petra and populating properties in Petrel within a 3D geocellular grid after a geological model construction is complete.

4.1 Log Analysis

4.1.1 Gamma Ray Log Normalization

The GR response to the rocks is affected by borehole surface casing, borehole size, mud weight, tool type and poor calibration. These factors can lead to biased logs and information about these factors is needed for explicit correction of the GR log; for example, caliper log and mud weight are needed to apply borehole correction. When such information is unknown, the usual solution is to use the GR value as-is, or apply GR log normalization to reduce systematic error caused by these factors.

In its simplest form, GR log normalization is based on the following two assumptions:

- All the clean sandstones in a study area have the same GR log reading, and all the pure shales have the same GR values;
- There is a clean sand interval and a pure shale interval in each well in the zone of interest and there are no major geological reasons for the GR values to vary across space.

GR log normalization transforms the biased logs so that the normalized GR values in the clean sandstone and the pure shale are equal to the specified reference values for the sandstone and shale. The equation is:

GR_nrm = GR_sand + (GR - GR_low) * (GR_shale - GR_sand) / (GR_high - GR_low)

Where:

GR_nrm = normalized gamma ray value

GR = input gamma ray value to be normalized

GR_sand = clean sandstone GR value to normalize to

GR_shale = pure shale GR value to normalize to

GR_low = clean sandstone GR value in the well to be normalized

GR_high = pure shale GR value in the well to be normalized

For regional mapping, the two assumptions mentioned above are rarely met. The workflow of GR log normalization was later generalized in Shier (2004). It involves taking the statistical average high and low values (reference values) from a type well within the zone of interest or averaged wells, and normalizing the biased log curve of other wells in the zone of interest (Shier 2004). The normalization becomes a process that translates and re-scales a biased log curve (not just GR) so that the spread and amplitude of the normalized histogram is similar to the histogram of the type well or averaged wells. Quartero et al. (2014) applied this process with a slight difference by deriving the reference high and low values from an analogous stratigraphic zone and then applying these values to the zone of interest, i.e., the cased interval of the well bore for through-casing GR log normalization.

Normalization was applied in this study to eliminate or reduce systematic bias caused not only by the surface casing, but also by other factors in an open hole. It differs slightly from Quartero et al. (2014) and includes the following steps:

a. For through-casing GR normalization, reference values were derived from the log for the open-hole portion of a well when it was available. The method of Quartero et al. (2014) was used only when the log for the open-hole portion was not available.
b. The reference value derived for the open-hole portion was then applied to the log for the cased interval of the same well; this process removed the bias caused by the surface casing only, and made the log from the cased interval consistent with the log from the open-hole portion of the same well. The normalized log from the cased interval and that from the open-hole portion of the same well were then merged as a single well path.
c. A statistical method was used to identify outlier logs from all the logs, including the normalized through-casing logs; and the identified outliers were corrected using normalization as described by Shier (2004).

4.1.1.1 *Define Intervals for Gamma Ray Log Normalization*

Prior to performing log normalization, four horizons were defined for each well; they are, in descending order, bedrock surface, shallow casing, the base of the Paskapoo and Porcupine Hills formations, and the base of the Scollard and Willow Creek formations. The bedrock surface was used to define the top limit of a log curve so that the Neogene–Quaternary sediments overlying the bedrock surface could be excluded from the analysis. The shallow casing defines the lower limit of the through-casing GR log. The shallow casing and the base of the Paskapoo and Porcupine Hills formations are used to define the upper and lower limits of the open-hole interval of the Paskapoo and Porcupine Hills formations. We used this interval to derive log statistics for normalization. When the shallow casing is within 50 m of the base of the Paskapoo and Porcupine Hills formations, the lower limit of the open-hole interval was set at the base of the Scollard and Willow Creek formations to ensure that adequate length of open-hole logs were used to derive reliable reference statistics.

4.1.1.2 *Through-casing Gamma Ray Log Normalization*

Statistics of the through-casing gamma log were computed and the values for the 5th percentile and the 95th percentile were obtained for every well that had a GR log through-casing.

For wells where the shallow casing is 50 m or more above the base of the Paskapoo or Porcupine Hills formations, the open-hole interval was defined as from the base of the Paskapoo and Porcupine Hills formations up to the shallow casing. Statistics for the GR log of the open-hole interval were calculated and the values for the 5th percentile and the 95th percentile were obtained for every well that also has a through-casing GR log. Wells located near the northeast margin of the study area tend to have a shallow casing that is less than 50 m above the base of the Paskapoo or Porcupine Hills formations. For these wells the open-hole interval is defined as from 50 m below the base of the Paskapoo and Porcupine Hills formations up to the shallow casing.

The through-casing GR log was normalized using the 5th percentile and the 95th percentile from the cased-hole portion as the low and high picks, and the 5th percentile and the 95th percentile from the open-hole portion of the same well as the reference low and high values.

The normalized through-casing GR log was then merged with that of the open-hole portion below for each well as a single well path.

4.1.2 Identify and Manage Outlier Gamma Ray Logs

The wells with the merged and normalized GR logs were pooled together with those that have the open-hole GR logs only. Statistics of the GR logs for each well for the interval from bedrock surface to the base

of the Scollard Formation were computed, including minimum, maximum, 5th percentile, 95th percentile, standard deviation, mean and median.

We examined the histograms of the minimum, maximum, 5th percentile, 95th percentile, standard deviation, mean and medium values. Wells with values located in the thin or flat portion of the two tails of each histogram were highlighted. The logs of these wells are referred to as outlier logs.

We then examined the outlier logs, and identified those that had a monotonous or constant value, a compressed or expanded range, and/or a biased mean. The biased logs and logs with a compressed or expanded range were corrected by normalization using the 5th percentile and the 95th percentile of the outlier wells as the low and high picks and the average of the 5th percentile and the 95th percentile for the zone as the targeted low and high reference values. Logs that could not be corrected were excluded from analysis.

The process was an iterative one, starting with identification of the first round of outliers using an arbitrary cut-off for the thin tails of the histogram. After removing bad logs and correcting biased logs using normalization, the statistics were recalculated, and the second round of outliers were identified based on the new histograms. The new outliers were then either removed or corrected using normalization. The process stops when it was determined that no obvious flat, very thin tails could be observed in the histograms.

4.1.3 Shale Volume Calculation

Linear estimation method for shale volume from the GR log was used and the equation is:

VSH_GR = (GR – GR_sand) / (GR_shale – GR_sand)

WHERE:

GR = gamma ray log reading in zone of interest

GR_sand = gamma ray log reading in l00% clean zone

GR_shale = gamma ray log reading in l00% shale

VSH_GR = shale percentage from gamma ray log

This method requires first determining the GR values associated with a zone of clean sandstone having no shale (GR_Sand) and a zone of 100% shale (GR_shale). In this project, these two values were chosen based on the statistics of GR values of the logs for the Paskapoo and Porcupine Hills formations. We chose 30 API as the GR value for GR_Sand, which is close to the mean of minimum GR values of the logs for the Paskapoo and Porcupine Hills formations. We chose 120 API as the GR_shale which is 30 API smaller than the mode of maximum GR values of the logs. This makes a 75 API GR log value correspond to 50% shale. This choice of the values of GR_sand and GR_shale makes our result potentially comparable with those of previous studies because the value of 75 API was used commonly as a cut-off threshold between sand-rich interval and shale interval (Lyster and Andriashek, 2012).

4.1.4 Density Logs Processing

Density logs taken through casing were excluded from the analysis. The open-hole density logs were examined and the outlier logs were dealt with using a similar process to that used for the GR logs, as described in Section 4.1.2.

In addition, density correction log was used to exclude density log values when the absolute density correction was greater than 0.15 gm/ cm^3.

4.1.5 Density Porosity Calculation

Total porosity was calculated from bulk density logs. The method used is based on a linear bulk mixing law and the equation is:

DPHI = (RHOMA - RHOB)/(RHOMA - RHOF)

Where:
RHOB = density log reading in zone of interest
RHOMA = density log reading in 100% matrix rock
RHOF = density log reading in 100% formation fluid
DPHI = total porosity from density log without shale correction

The method requires density values for both the matrix (RHOMA) and formation fluid (RHOF). The sandstones of the Paskapoo Formation consist of framework grains including quartz, feldspar, and rock fragments (mainly chert, volcanic, metamorphic and sedimentary rock fragments) (Grasby et al., 2007, 2008) and are typically classified as litharenites based on Folk's classification (Folk, 1968). As a result the sandstone scale matrix density, 2.65 g/cm^3, cannot be used and a new matrix density needs to be calculated. Also, the density of the matrix and formation fluid would change over such a large region under study.

Unfortunately, distributions of both matrix and fluid density are very difficult to estimate over such a large area and adequate information to do so is not available. The neutron-density cross plot of 1 236 wells confirms that the matrix is not pure quartz and the matrix density for the zone with a GR value less than 50 API is 2.77 g/cm^3 (Figure 5). This value was used as the new matrix density. The fluid density was set as 1 g/cm^3.

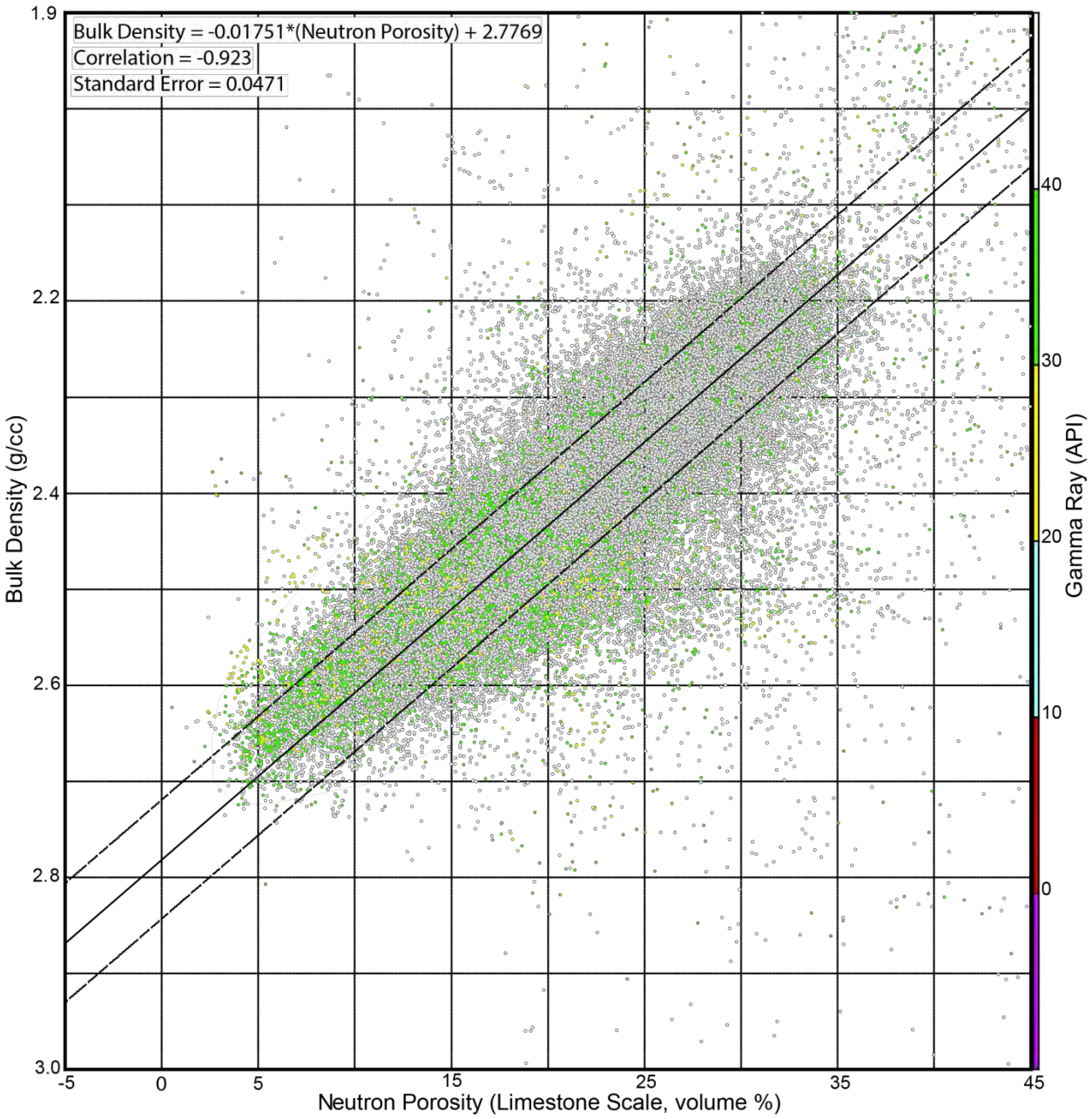

Figure 5. Neutron-density cross plot of 1 236 well logs, filtered by gamma ray <50 API.

No shale volume correction was applied to the calculated total porosity because the histogram of the porosity of shale (>=120 API) indicates that it has the full range of the porosity of the entire Paskapoo Formation and varies considerably over the study area. This makes it impossible to get a constant porosity value for the pure shale that is required for a shale volume correction of porosity.

5 3D Modelling in Petrel

5.1 Input Source Data

The input source data for the 3D modelling included shale percentage logs derived from GR logs, coded shale percentage logs derived from water well lithological descriptions, porosity logs derived from bulk density logs, and geological framework surfaces. Figure 6 is a cross-section showing an example of the well logs and surfaces. The shale percentage logs were obtained from 29 429 oil and gas wells, the density porosity logs were from 13 611 oil and gas wells, and the coded shale percentage logs were from 86 184 water wells. The geological framework surfaces were from version one of the 3D Provincial Geological Framework Model of Alberta (Branscombe et al., 2018) and include, in ascending order, the surface for the base of the Scollard Formation, the surface for the top of the Scollard Formation that defines the base of the Paskapoo and Porcupine Hills formations and the erosional portion of the top of the Scollard Formation, and the bedrock topography surface.

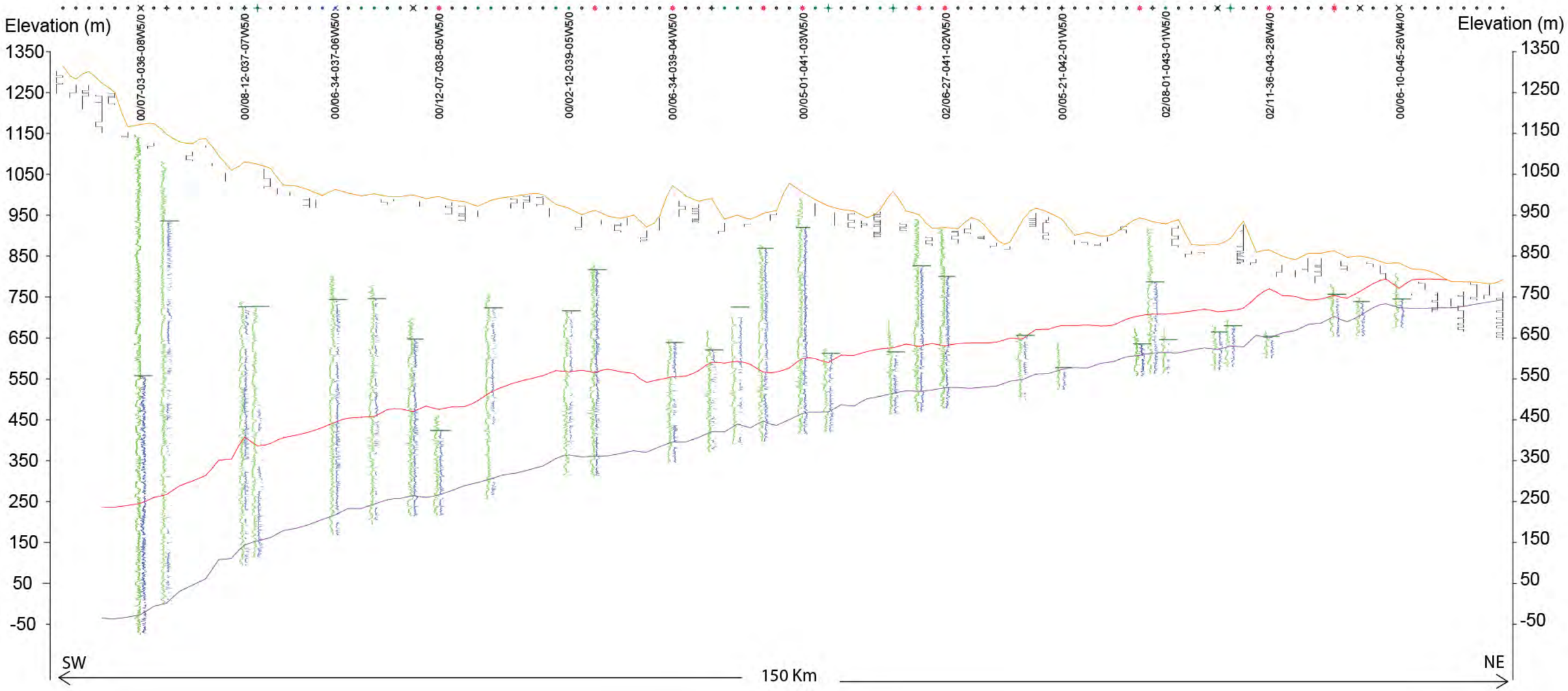

Figure 6. Well log cross-section along line 3 in Figure 1. Logs: black is the coded shale percentage log from water wells; green is the shale percentage log from oil/gas wells; blue is the density porosity log. Horizons: orange is KB; the bedrock surface is close to the KB and not shown here because it blocks the coded shale percentage log; red is the base of the Paskapoo Formation; purple is the base of the Scollard Formation. Dark green bars indicate the base of surface casing. Top row are oil/gas well and water well symbols, and only selected oil/gas wells are labelled.

5.2 Structural Framework

The structural framework of the 3D model was created in Petrel using the 3D Simple Grid tool. Three geological framework surfaces (the base and top surfaces of the Scollard Formation and the bedrock surface) were used to make three 3D property model horizons. These horizons define two zones in the 3D property model: the Scollard Formation zone and the Paskapoo and Porcupine Hills formations zone. The extent of the 3D property model is defined by the extent of the base surface of the Scollard and Willow Creek formations. We set the horizontal grid increment to 500 m x 500 m and divided the structural model vertically into layers to create a 3D geocellular model. The layers were created using the follow base option for the Paskapoo and Porcupine Hills formations and set to nominally 5 m thick, with some layers being thinner where they are pinched out by the top model horizon approaching the base model horizon to the east margin. For the Scollard and Willow Creek formations, the layers were created using the proportional layering option with the averaged layer thickness close to 5 m. At a horizontal grid of 500 m x 500 m and a vertical grid of nominally 5 m, the 3D geocellular model has 1027 x 1343 x 273 cells for a total of 376 538 253 grid cells, 34 666 066 of which defined the property values.

5.3 3D Property Modelling

The shale percentage and density porosity were modelled using geostatistical methods to populate the 3D geocellular model. The 3D property modelling included five steps:

- Upscale the well log data to the scale of the 3D geocellular grid.
- Transform the upscaled data to a normal score distribution.
- Calculate the experimental variograms for each normal score transformed variable.
- Fit variogram models to the experimental variograms.
- Populate the 3D geocellular grid using a geostatistical algorithm.

5.3.1 Upscale and Transform Well Log Data

The well log data for the shale percentage and density porosity was recorded at very fine regular intervals (typically 6” or 15.2 cm) and the coded water well data were resampled at 10 cm intervals. To model these properties in a 3D model where the cells are 500 x 500 x 5 m, the data were upscaled from the well logs to the geocellular model to facilitate the property modelling. In the upscaling process, the averaging of a data set from a scale of 15.2 cm to 5 m reduces the variance of the data distribution as the highest and lowest values are smoothed out.

A normal score transformation was applied to the upscaled well log data. This transformation makes the upscaled data follow a standard normal (Gaussian) distribution with a mean of zero, a variance of one, and a normal or bell-curve distribution. A back transformation restores the shape and units of the input distribution from the upscaled data values after the modelling is completed.

5.3.2 Variogram Modelling

The geostatistical method used for property modelling requires the spatial structure of the modelled variable to be quantified (Pyrcz and Deutsch, 2014). A variogram quantifies the relationship between values at specified distances and this information is used to calculate the weights for data points used for estimation. An experimental variogram is calculated from data and then a variogram model function is fitted. For 3D property modelling, the variogram needs to be calculated and modelled in three directions: the major and minor horizontal directions, and the vertical direction. Each direction is modelled independently of the others, but with the same nested structures in the function.

A variogram model was needed for each variable in each zone or facies. Using shale percentage in the Paskapoo/Porcupine Hills zone as an example, variograms were calculated and modelled using a spherical function with the major direction of horizontal correlation at an azimuth of 135 degrees and the minor direction perpendicular to that.

Figure 21 shows the experimental and modelled variograms for shale percentage in the Paskapoo/Porcupine Hills zone. The vertical direction displays zonal anisotropy; and the variogram does not appear to reach the sill of 1.0 for a very long distance. A structure with a very short horizontal range was used to account for this. There is an apparent nugget effect in the horizontal directions that is higher than the apparent sill in the vertical direction. A structure with a short horizontal range was used to account for this. Both the major and minor horizontal directions show slight zonal anisotropy; as a result, a structure was used to capture the partial sill of the zonal anisotropy of the major and minor horizontal directions and another structure for the rest of the apparent sill.

Figure 22 shows the experimental and modelled variograms for shale percentage in the Scollard zone. Table 1 shows the parameters for the shale percentage variable modelling. Figures 23 and 24, and Table 2 show the experimental and modelled variograms, and parameters for the density porosity variable modelling. Figure 25 and Table 3 show the experimental and modelled variograms and parameters for the shale percentage variable derived from water wells.

5.3.3 Populate 3D Geocellular Grid

In this study we used the Gaussian Random Function Simulation (GRFS) (Daly et al., 2010) in Petrel for property modelling. This geostatistical method is based on kriging (Pyrcz and Deutsch, 2014) to estimate the values and then adds an unconditionally simulated random value to the kriging estimates to generate a realization that is conditional to the input data and correctly reproduces the variability in the original data.

Cosimulation was used for the shale percentage variable to incorporate the coded water well data as a secondary variable. This accounts for the correlation between the coded water well data and the GR logs, and was used because there is much more water well data than GR data for the interval of less than 150 m in depth. Cosimulation was accomplished by first finding the correlation coefficient between the GR derived shale percentage and the water well derived shale percentage. The coefficient was found to be 0.26. Then, a model of water well derived shale percentage was created using the simple kriging algorithm. Finally, the shale percentage model was created by using GRFS, using the collocated simple co-kriging method. The shale percentage derived from GR logs was the primary variable and the model of water well derived shale percentage was the secondary variable. One hundred realizations were generated to capture the full range of uncertainty for the shale percentage variable.

Figures 7 and 8 show isometric views of two simulated realizations of the shale percentage model, the arithmetic mean of 100 realizations and the kriged model. Each realization is different, but equally probable and honours all of the data. The simulated realizations typically look “patchy” with a mixture of high and low values; however, the arithmetic mean of 100 realizations is smooth and nearly identical to the kriged model, with cell values tending towards the centre of the distribution.

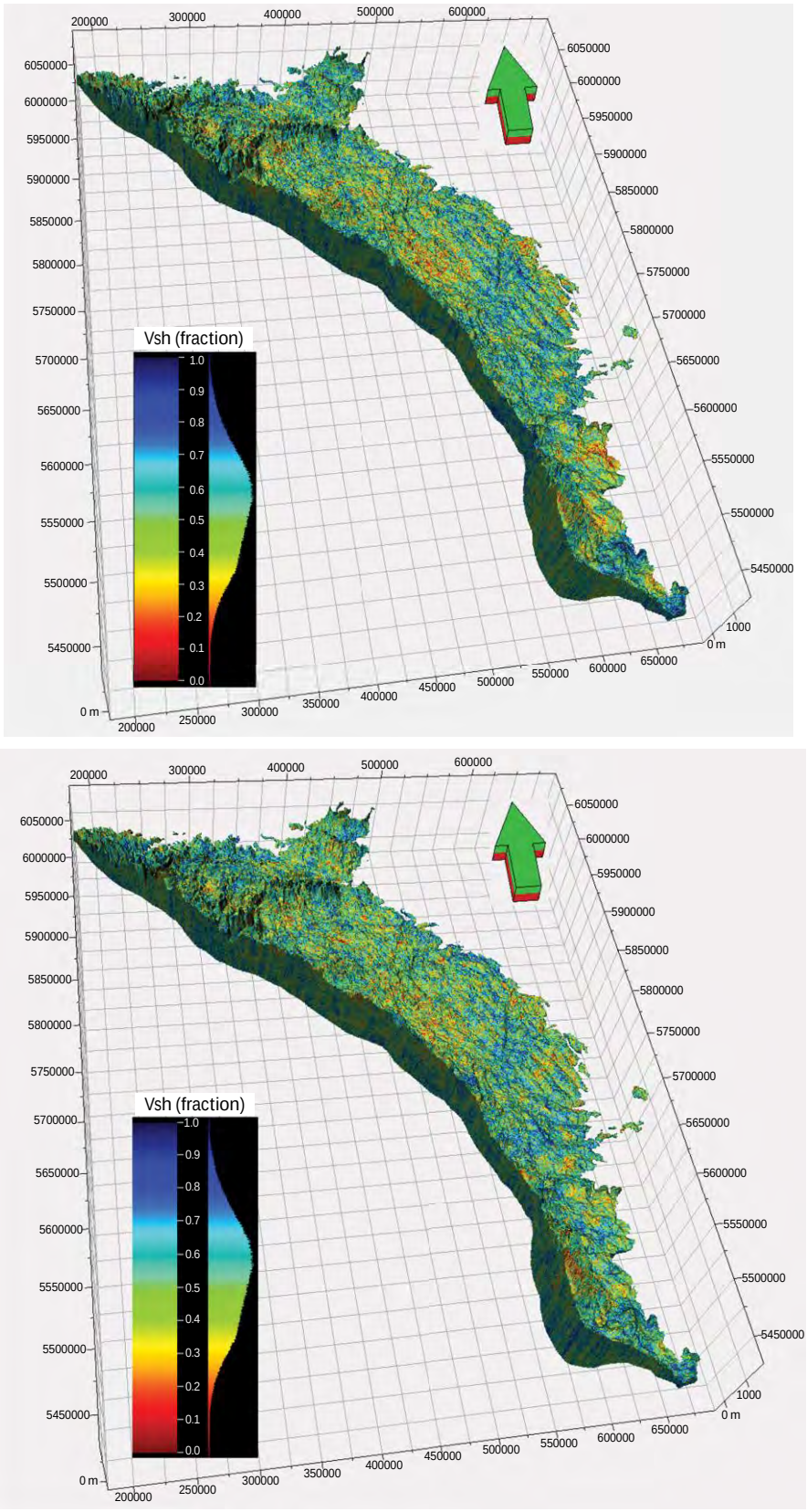

Figure 7. Isometric view of two realizations for the shale percentage model. Vertical exaggeration is 50 times.

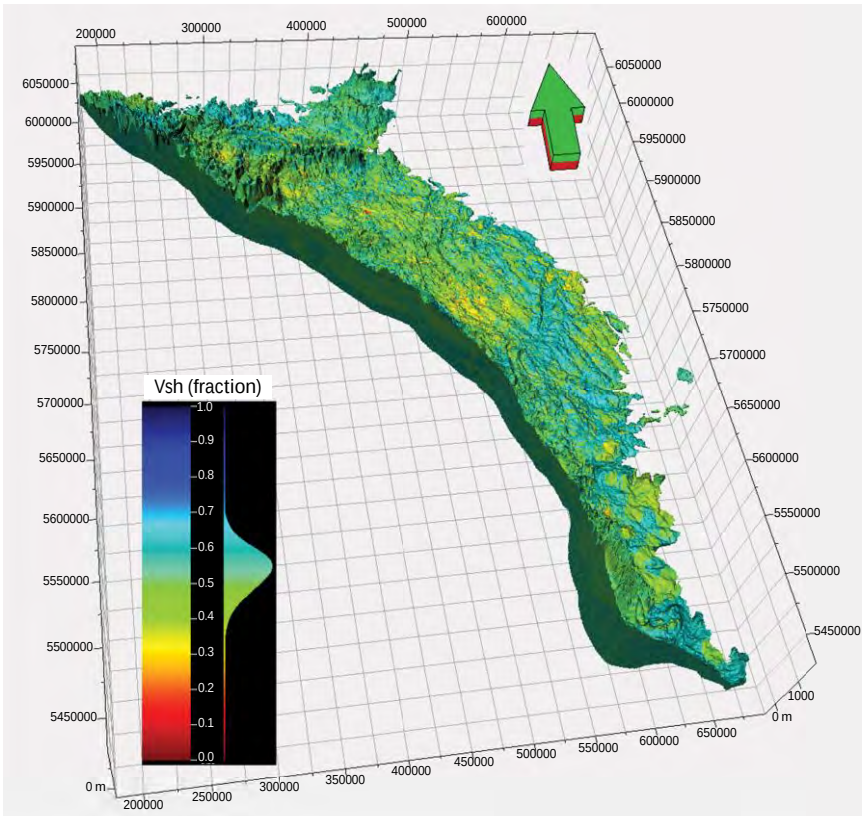

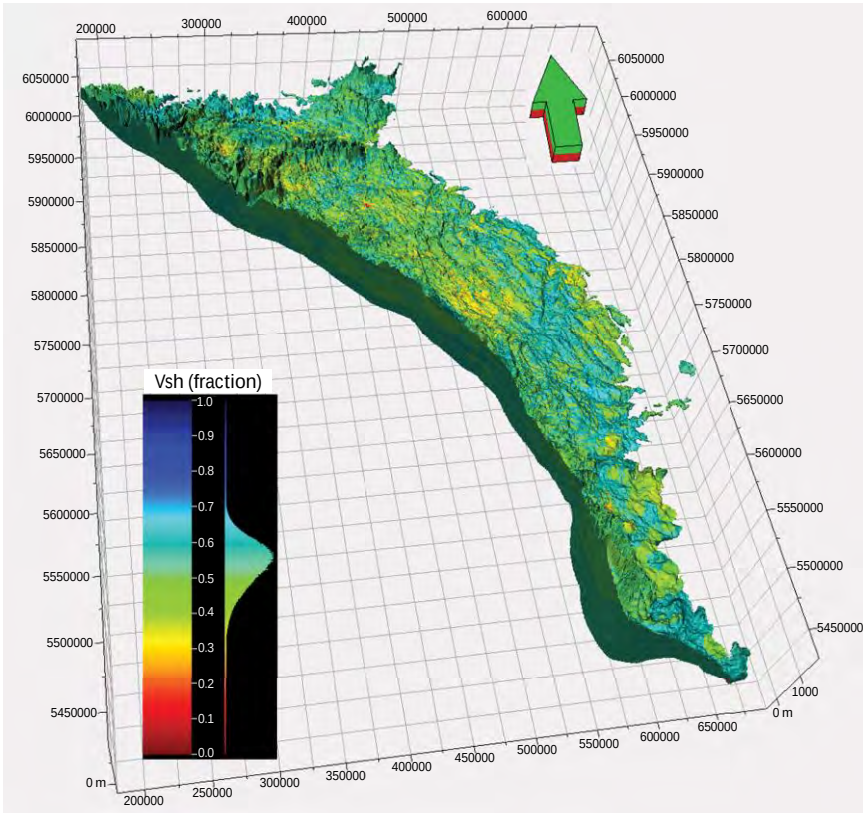

Figure 8. Isometric view of the arithmetic mean of 100 realizations (top) and the co-kriging model (bottom) for the shale percentage model. Vertical exaggeration is 50 times.

The 100 simulated realizations allow the 10th percentile (P10) and 90th percentile **(**P90) to be calculated for each cell in the 3D model. Figure 9 shows the isometric views of the P10 and P90 models. The P10 model is commonly used to highlight areas with a high possibility of high values because 90 out of 100 models predicted that the shale percentage values could exceed the value at any locations in the P10 model. The P90 model is commonly used to highlight areas with a high possibility of low values because 90 out of 100 models predicted that the shale percentage values could be less than the value at any locations in the P90 model. For example, the central-west area of the model is represented as green (relatively low shale percentage) in the P90 model, indicating that the area is more certain to be sandstone-dominated compared to other areas. To the southeast of this region is an area represented by green (relatively high shale percentage) in the P10 model, indicating that this area is more certain to be shale-dominated compared to other areas (Figure 9).

Figure 10 shows the isometric view of the fence diagram of the kriged model of the shale percentage to show how it varies regionally throughout the model area.

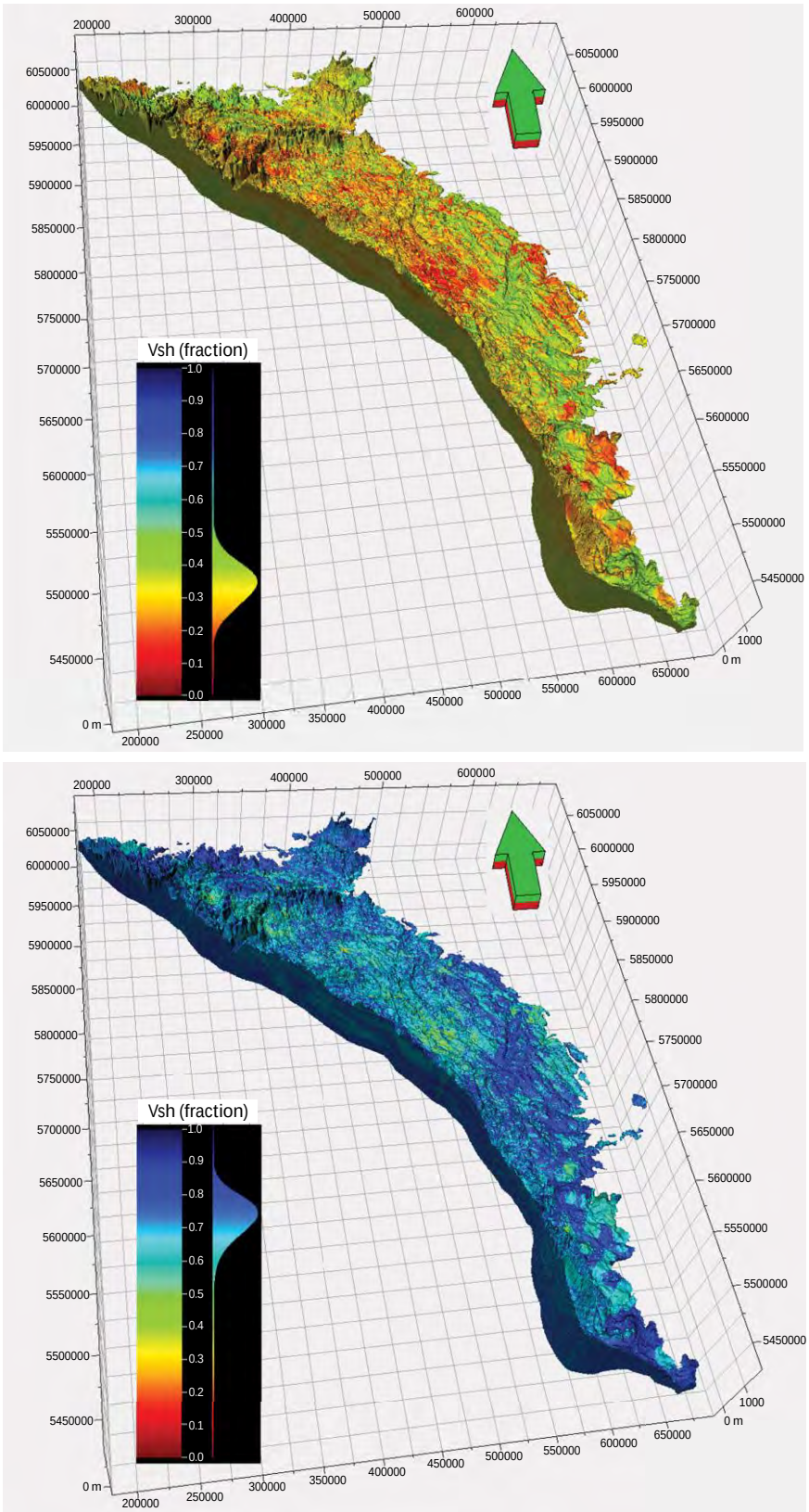

Figure 9. Isometric views of the 10th (top) and 90th (bottom) percentiles for the shale percentage model. Vertical exaggeration is 50 times.

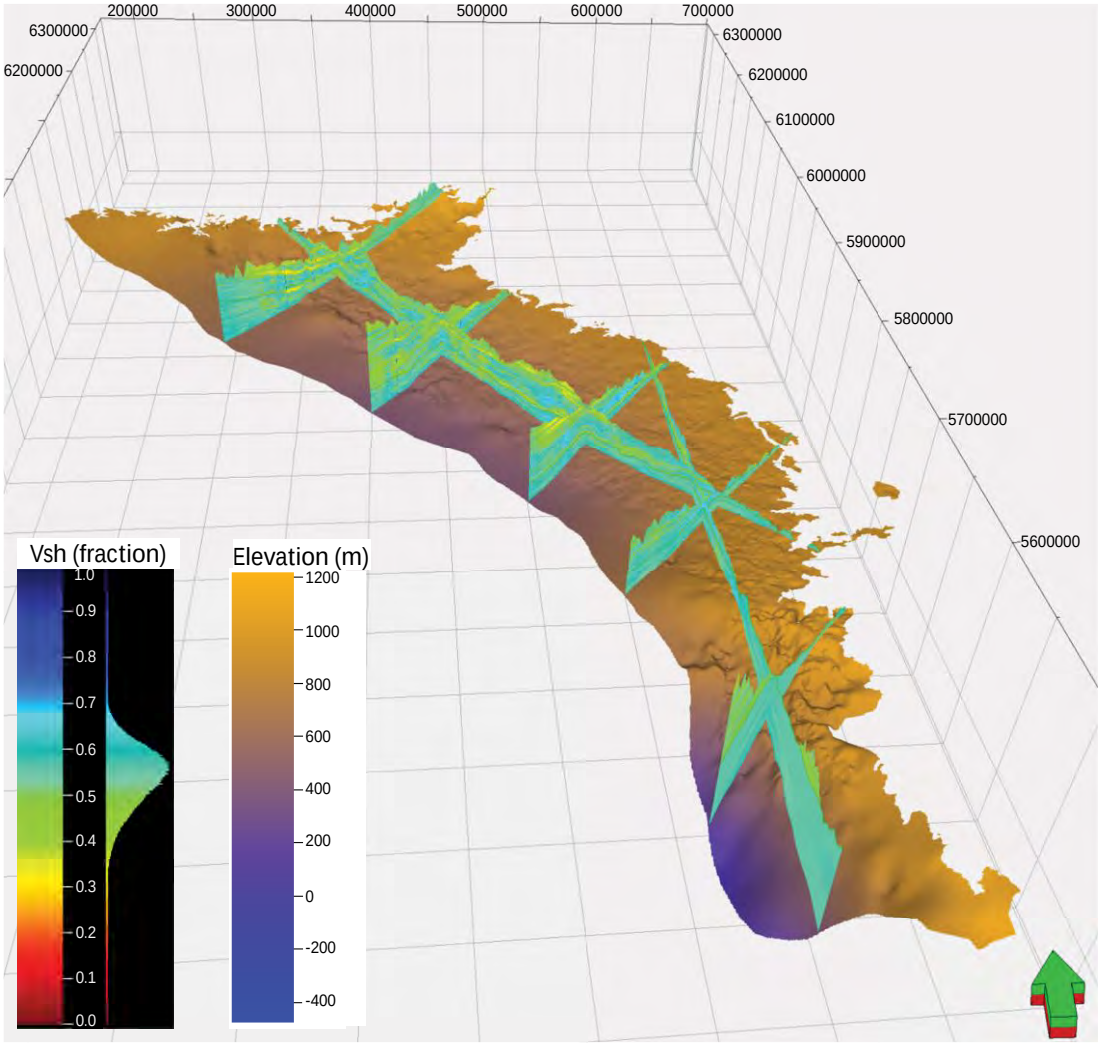

Figure 10. Isometric view of the fence diagram of the kriged shale percentage model. Locations of the cross-sections are indicated by lines 1–7 in Figure 1. The surface at the base of the fences is the base of the Scollard and Willow Creek formations. Vertical exaggeration is 50 times.

For the density porosity model, cosimulation was used with porosity as the primary variable and shale percentage as the secondary variable. This accounts for the correlation between the two variables and takes advantage of the fact that there is much more oil/gas GR data than density porosity data for the interval above the surface casing near the ground surface. The correlation coefficient between the normal score transformed shale percentage variable and density porosity variable was found to be -0.01. One hundred realizations were generated to capture the full range of uncertainty for density porosity and every active cell in the 3D model was simulated for every realization.

Figures 11 and 12 show isometric views of two simulated realizations of the density porosity model, the arithmetic mean of 100 realizations and the kriged model. Each realization is different but equally probable and honours all of the data. The simulated realizations typically look “patchy” with a mixture of high and low values; however, the arithmetic mean of 100 realizations is smooth and nearly identical to a kriged model, with cell values tending towards the centre of the distribution (Figure 12).

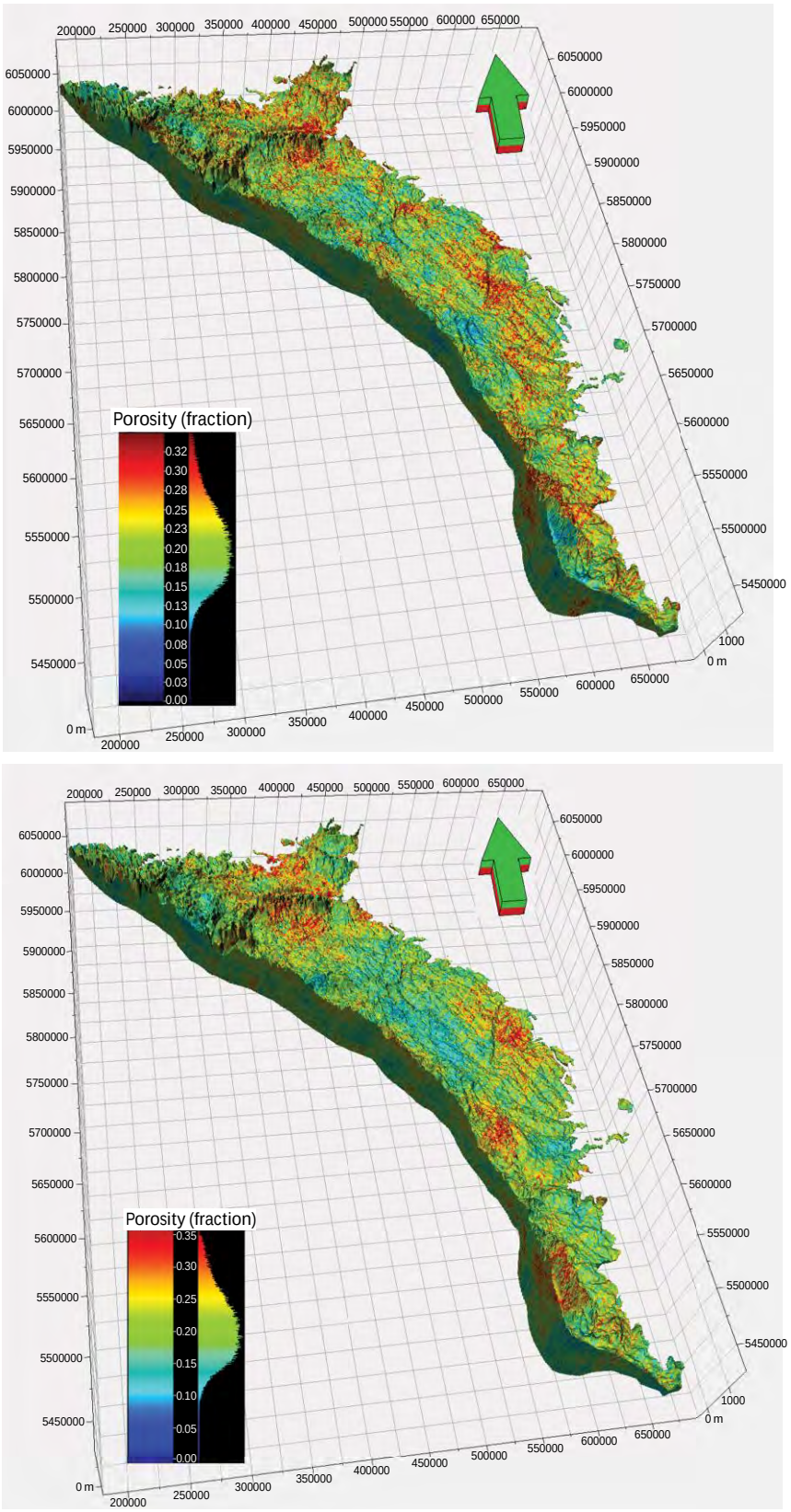

Figure 11. Isometric view of two realizations for the density porosity model. Vertical exaggeration is 50 times.

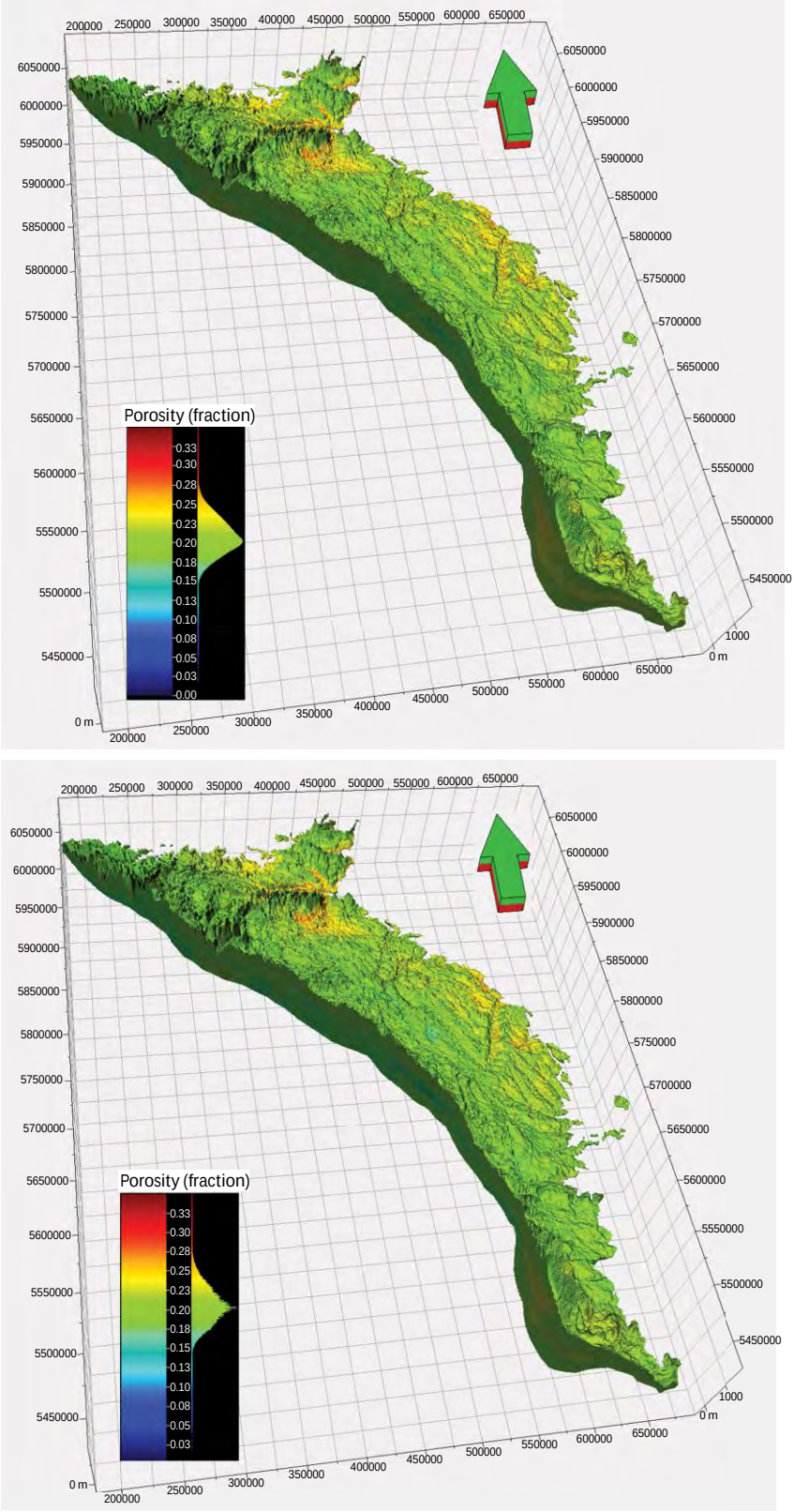

Figure 12. Isometric view of the arithmetic mean of 100 realizations (top) and the co-kriging model (bottom) for the density porosity model. Vertical exaggeration is 50 times.

Figure 13 shows the isometric views of the 10th percentile (P10) and 90th percentile (P90) models of the density porosity. These two maps indicate that the northeast region of the model is more certain to be porous compared to the southwest region. Figure 14 is an isometric view of the fence diagram of the kriged model to show how the porosity varies regionally throughout the model area.

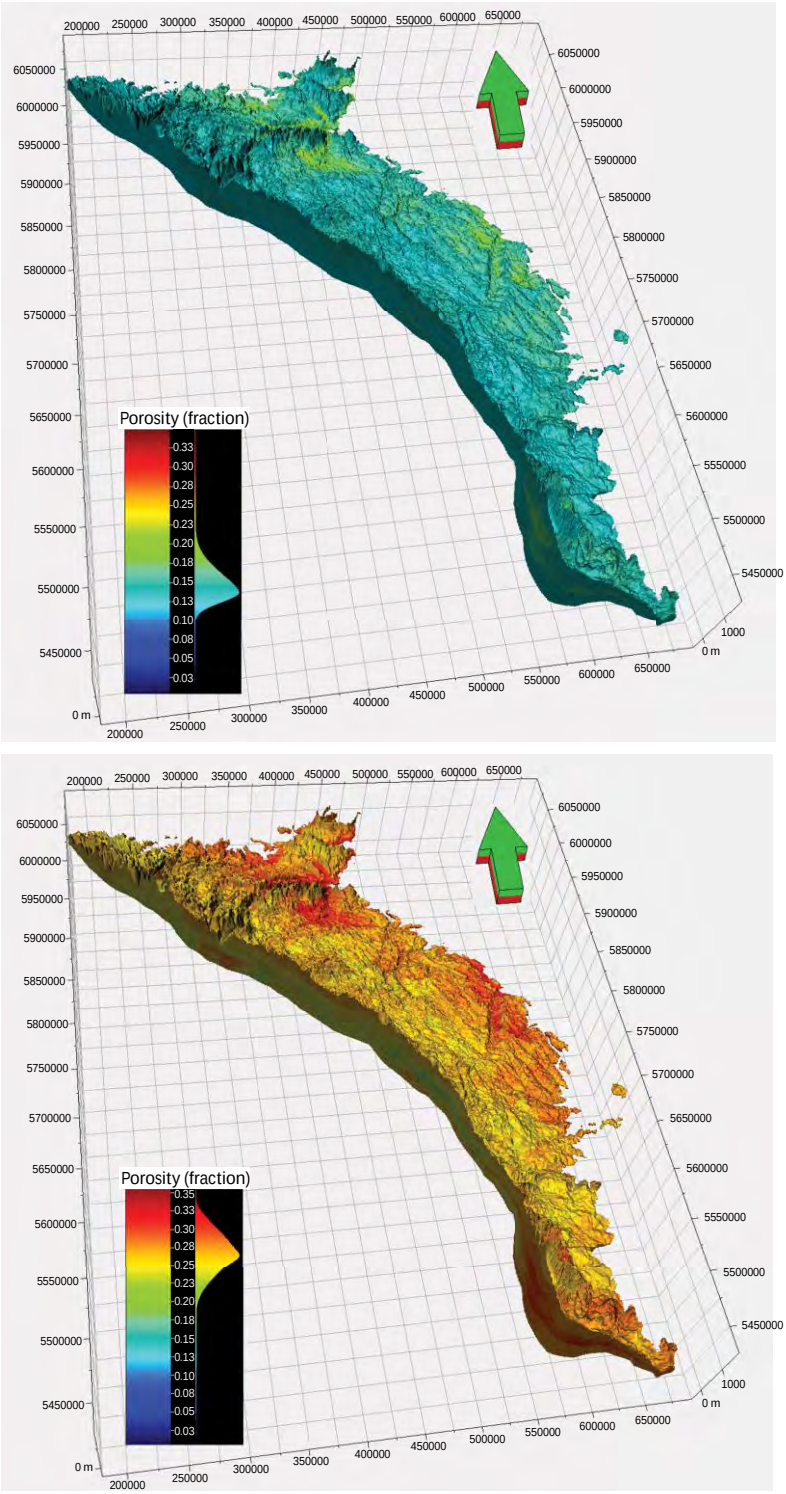

Figure 13. Isometric view of the 10th (top) and 90th (bottom) percentiles for the density porosity model. Vertical exaggeration is 50 times.

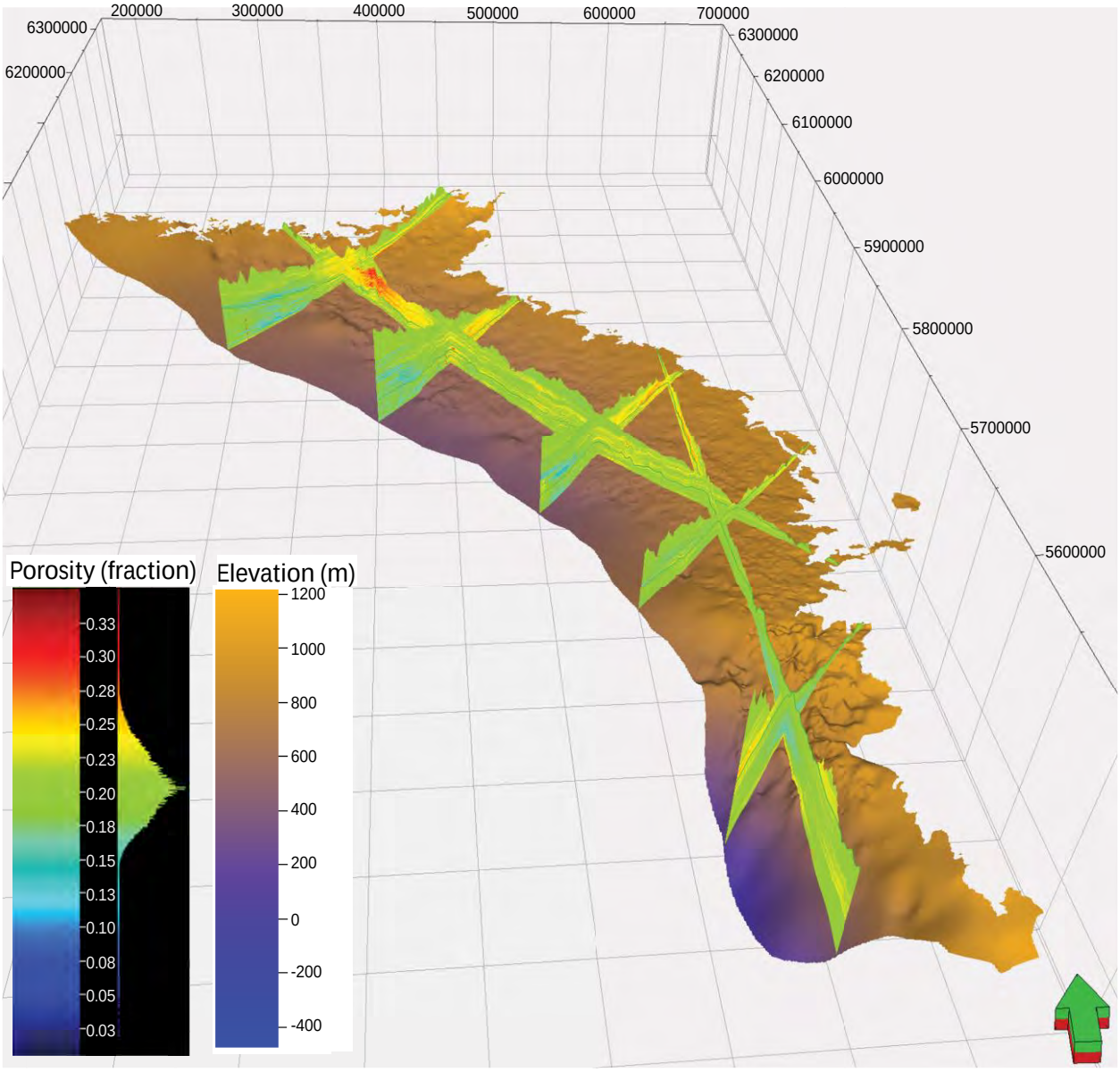

Figure 14. Isometric view of the fence diagram for the density porosity model. Locations of the cross-sections are indicated by lines 1–7 in Figure 1. The surface at the base of the fences is the base of the Scollard and Willow Creek formations. Vertical exaggeration is 50 times.

6 Model Quality

As mentioned previously, the model of shale percentage was developed from two different types of data: GR logs from oil/gas wells and lithological descriptions from water wells. The model of porosity was developed from density logs. The uncertainty of the 3D model is dependent on the quality of these input data and choices made during analysis and modelling.

The normalization, applied to through-casing GR logs and some of the outlier GR logs, helps to reduce the systematic bias of the GR logs, but will not remove the random error associated with the GR logs, and the systematic bias cannot be completely removed. In calculating the shale percentage, a single GR cut-off value of 30 API for the pure sandstone member and a single cut-off value of 120 API for the pure shale member were arbitrarily chosen and used across the entire region of the Scollard and Willow Creek formations. This is not perfect; however it is the closest assumption that was possible for such a large-scale model. The

variation in the GR response to the pure sandstone and pure shale over such a large region will contribute to reducing the trueness to reality for the calculated shale volume or sandiness.

Density logs were only used below the surface casing, thus reducing the confidence level due to the limited quantity of data for the interval above the base of the surface casing. In calculating the porosity, a single grain density value of 2.77 g/cm^3 and a single fluid density value of 1 g/cm^3 were used across the entire region of the Scollard and Willow Creek formations. This reduces the trueness to geological complexity and reality. Although the range and mean (21%) of the calculated total porosity are close to those of previous studies (e.g., 19.2% by Grasby et al., 2007, and 23.2% by PRCL, 2014), the matrix grain density value of 2.77 g/cm3 derived from the neutron-density cross-plot placed it into the area between the calcite line and the dolomite line on the cross-plot (Figure 5). This density value may appear to be higher than the unknown, true average value of the matrix grain density for the entire study area and, as a result, the calculated porosity may appear to be inflated; however, the regional trend and pattern of porosity distribution revealed for the study area remain intact due to the fact that the trend is dependent on differences between different areas and not dependent on the absolute value at each location.

A sensitivity analysis, obtained by taking the partial derivative of the response equation of density porosity with respect to matrix density and fluid density respectively, indicates that for a water-filled sandstone with a 30 % porosity, an error of 0.05 g/cm^3 in the supposed matrix density will only alter the calculated porosity by 2 %, and a variation of more than 0.1 g/cm^3 in the fluid density corresponds to a similar 2% error in the calculated porosity. This is fortunate because a single estimated value for the matrix density and a single estimated value for the fluid density can still be helpful in revealing the regional trend of porosity.

The coded lithological data from the water well descriptions are numerous, but are available only for the near-ground surface interval above 150 m in depth. Also, the water well data is generally lower quality compared to the oil/gas well log data, and therefore were used as a secondary variable for the property modelling.

The base of the Scollard and Willow Creek formations and the base of the Paskapoo and Porcupine Hills formations were adopted from version one of the 3D PGF (Branscombe et al., 2018) and the uncertainty associated with these surfaces will propagate into the modelling process and impact the quality of the 3D property model. In the construction of the model the following base option was used for the Paskapoo and Porcupine Hills formations and in property modelling the data used for interpolation was declustered by layer, meaning that neighbour data points within the same layer as the point to be estimated were preferentially used. Having high accuracy geological surfaces ensures that the data points used for interpolation were from rock deposited during the same time. The uncertainty of the surfaces is higher to the south and northwest because few or no data are available and these portions of the surfaces were extrapolated; this led to a higher uncertainty of the model in these areas (Figure 15).

The uncertainty associated with the modelling was presented as the kriging standard deviation for each voxel in the model, which was calculated from the 100 realizations from simulation. Figure 15 shows the uncertainty for the shale percentage model and the density porosity model.

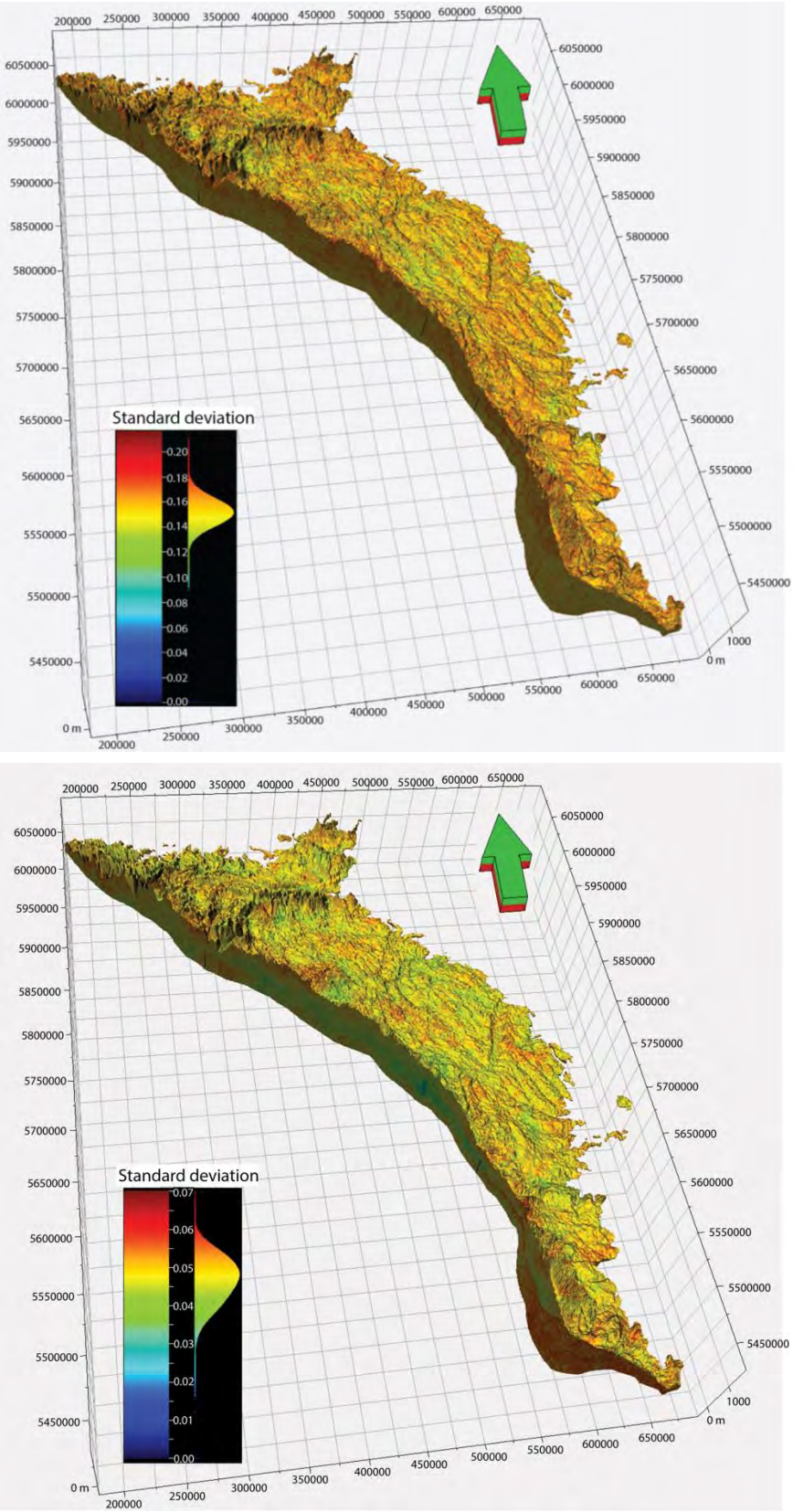

Figure 15. Isometric view of the kriging standard deviation for the shale percentage model (top) and the density porosity model (bottom). Vertical exaggeration is 50 times.

The 3D model developed for this study is appropriate only for regional-scale use (1:100 000). This model is not intended to be used for site-specific investigations because its accuracy is constrained by the data quality, quantity, distribution, and geological complexity at a regional scale.

7 Observations

The 3D property model illustrates a wide variation in sandstone abundance in the near-surface Paskapoo, Porcupine Hills, Scollard, and Willow Creek formations in southwest Alberta. Several regional trends are apparent from the shale percentage model:

- A basal sandstone unit (~50 m thick) within the Paskapoo Formation is well developed in the central part of the study area (Figure 16), however, it grades into mudstone or becomes discontinuous and absent in the northern and southern parts of the study area (Figure 16).
- Above the basal sandstone unit of the Paskapoo Formation is an interval of mudstone (low sandstone abundance) (~300 m thick) in the middle part of the Paskapoo Formation (Figure 16). It grades into an interval of slightly higher sandstone abundance towards the central west (Figure 16).
- The mudstone interval in the middle part of the Paskapoo Formation grades into an interval of higher sandstone abundance in the upper portion of the Paskapoo Formation (Figure 16).
- The Porcupine Hills Formation in the southwest of the study area does not show the three-layer structure as observed for the Paskapoo Formation. Instead, it is characterized by a sandier interval in the lower part and a mudstone and siltstone interval for the middle and upper part of the formation (Figure 17).
- The Paskapoo Formation has an average 53% shale volume and higher abundance of sandstone units compared to the Scollard Formation which has an average of 55% shale volume (Figures 16 and 17).

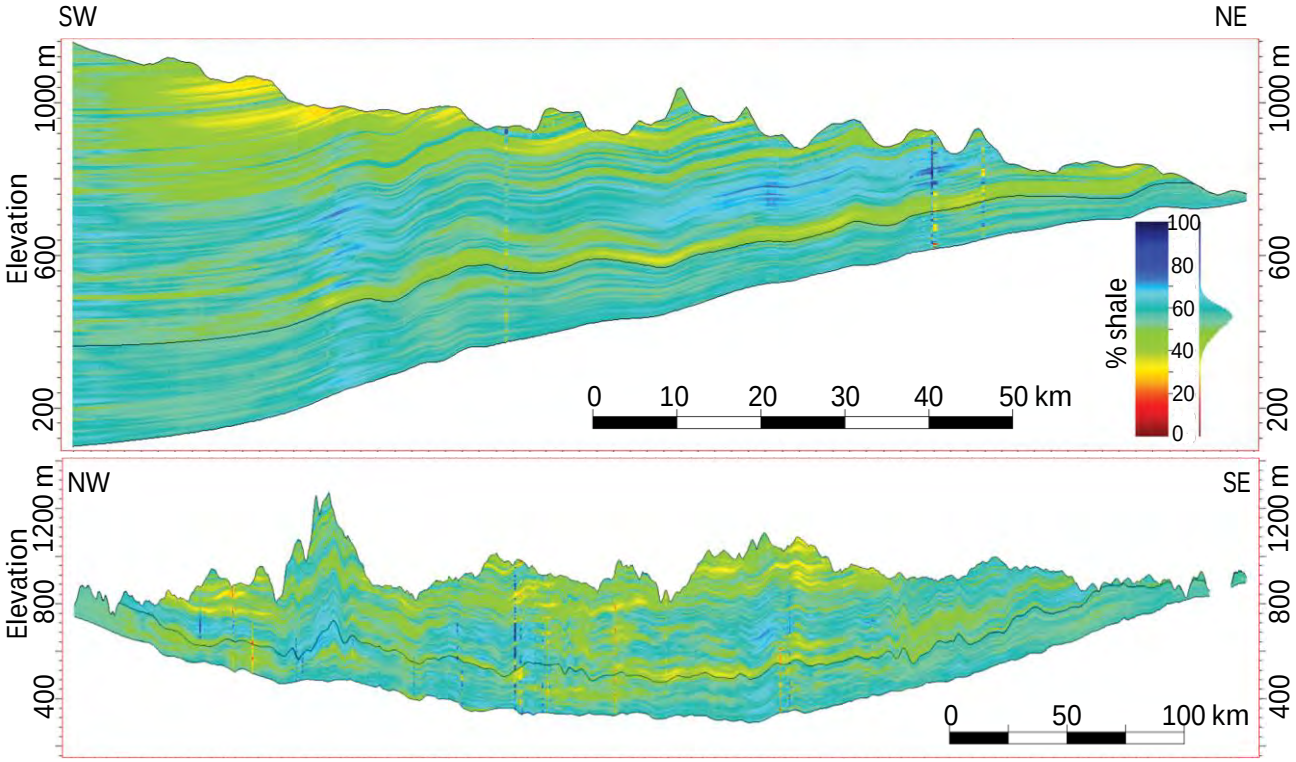

Figure 16. Cross-sections of the kriged shale percentage model. The black line across the cross-section indicates the boundary between the Paskapoo Formation and the Scollard Formation. The cross-section locations are shown by line 3 and line 6, respectively, in Figure 1. Vertical exaggeration is 45 times (upper) and 100 times (lower).

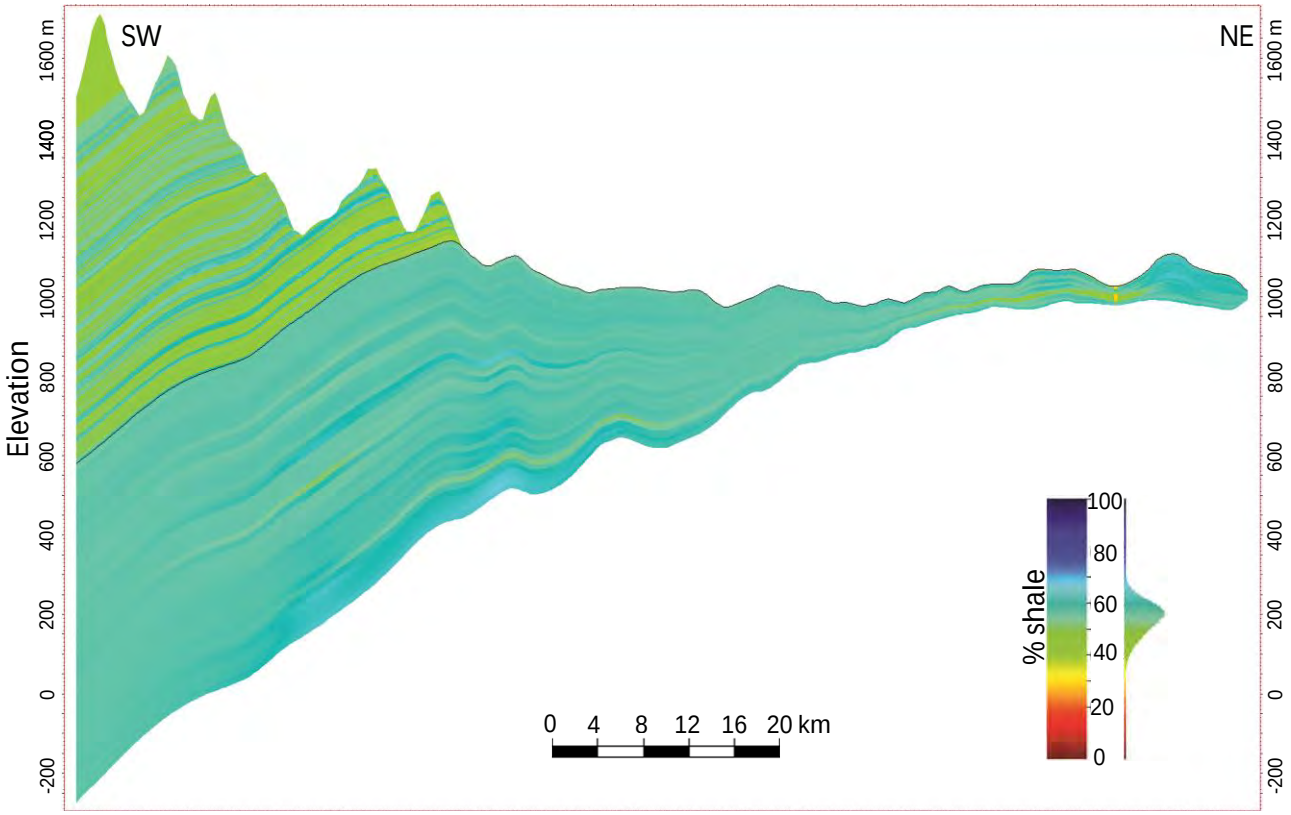

Figure 17. Cross-section of the kriged shale percentage model. The black line across the cross-section indicates the boundary between the Paskapoo Formation and the Scollard Formation and the eroded top of the Scollard Formation. The cross-section location is shown by line 5 in Figure 1. Vertical exaggeration is 35 times.

The shale percentage model confirms: 1) the three-layer subdivision for the Paskapoo Formation as proposed by Demchuk and Hills (1991); 2) the presence of abundant sandstone of the Sunchild aquifer in the northwest part of the study area (Figure 16), which is often exposed along the Athabasca River; 3) the extensive and thick basal sandstone unit (i.e., Haynes aquifer) in central part of the study area is absent in the northwest of the study area (Figure 16), as suggested by (Quartero et al., 2015).

Several regional trends were observed from the density porosity model (Figure 18):

- The density porosity generally increases up-dip from west to east for both the Scollard Formation and the Paskapoo Formation; this is also indicated by the variograms in the minor direction for both the Scollard Formation and the Paskapoo/Porcupine Hills formations, which show a clear trend above the sill (see Figures 23 and 24) in the minor directions.
- The density porosity is higher in the northern part than in the southern part of the study area (see Figure 18).
- The density porosity has a poor correlation with the shale percentage (compare Figure 16 and Figure 18)

Grasby et al. (2007) identified three types of porosity for the Paskapoo Formation: intergranular porosity, secondary porosity, and microporosity. Most sandstone was found to be grain supported with several pore-filling phases including authigenic clays (chlorite, kaolinite), calcite cement, and pyrite (Grasby et al., 2007). A bimodal permeability distribution was obtained for the Paskapoo sandstones (Grasby et al., 2007; Hughes et al., 2017). Qualitative thin-section analyses by Hughes et al. (2017) indicated that for sandstone units with similar grain size, a wide range in porosity values can arise owing to the amount of cementation and other pore-filling processes. Hughes et al. (2017) interpreted the disparity between the hydraulic properties of the

sandstone units of the Paskapoo Formation (i.e., Sunchild and Haynes aquifers) by hypothesizing that the porosity of the sandstones is governed by cementation rather than grain size. This may explain the poor correlation between the shale percentage variable and the density porosity variable (compare Figure 16 and Figure 18). However, further detailed study is needed to understand the complex relationships among lithology, diagenesis, and porosity.

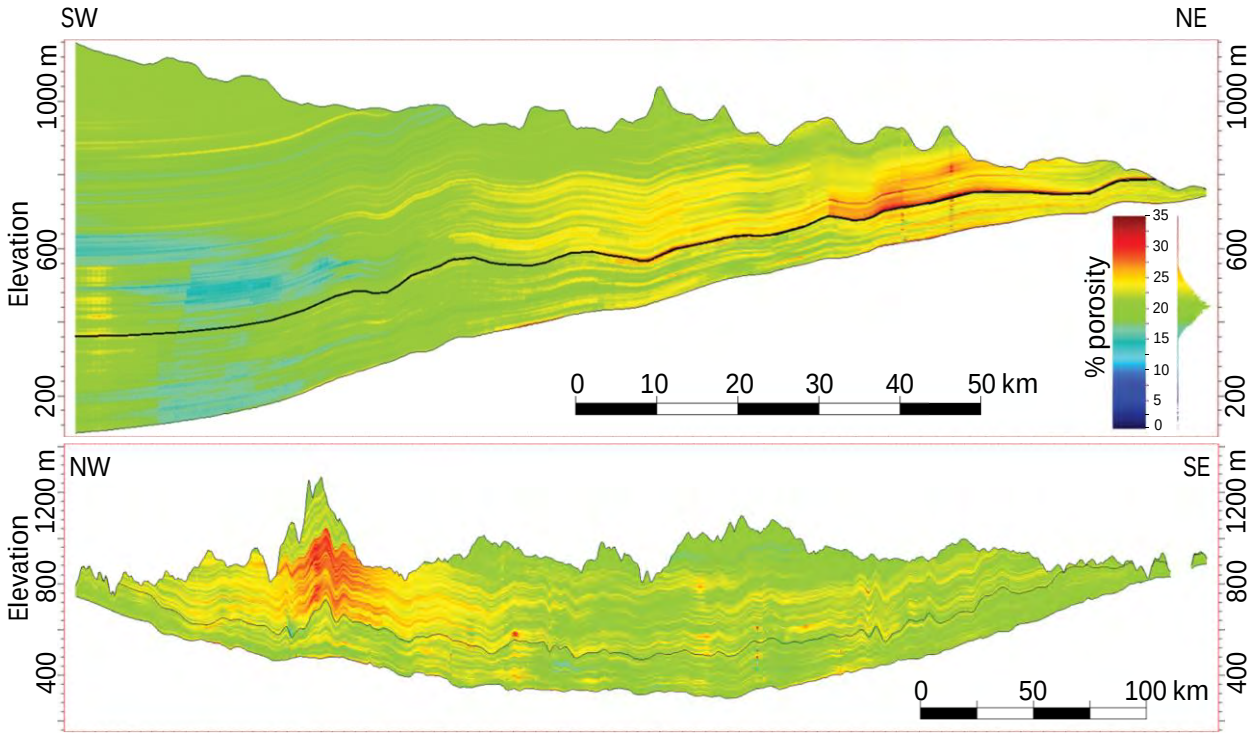

Figure 18. Cross-sections of the kriged density porosity model. The black line across the cross-section indicates the boundary between the Paskapoo Formation and the Scollard Formation. The cross-section locations are shown by line 3 and line 6, respectively, in Figure 1. Vertical exaggeration is 45 times (upper) and 100 times (lower).

8 Summary and Discussion

The 3D property model developed for this study illustrates at a higher resolution compared to previous studies (Figure 19) the degree of heterogeneity of shale percentage and porosity in the near-surface bedrock of southwest Alberta. The model is appropriate only for regional-scale use (1:100 000) and not intended for use in place of site-specific investigations.

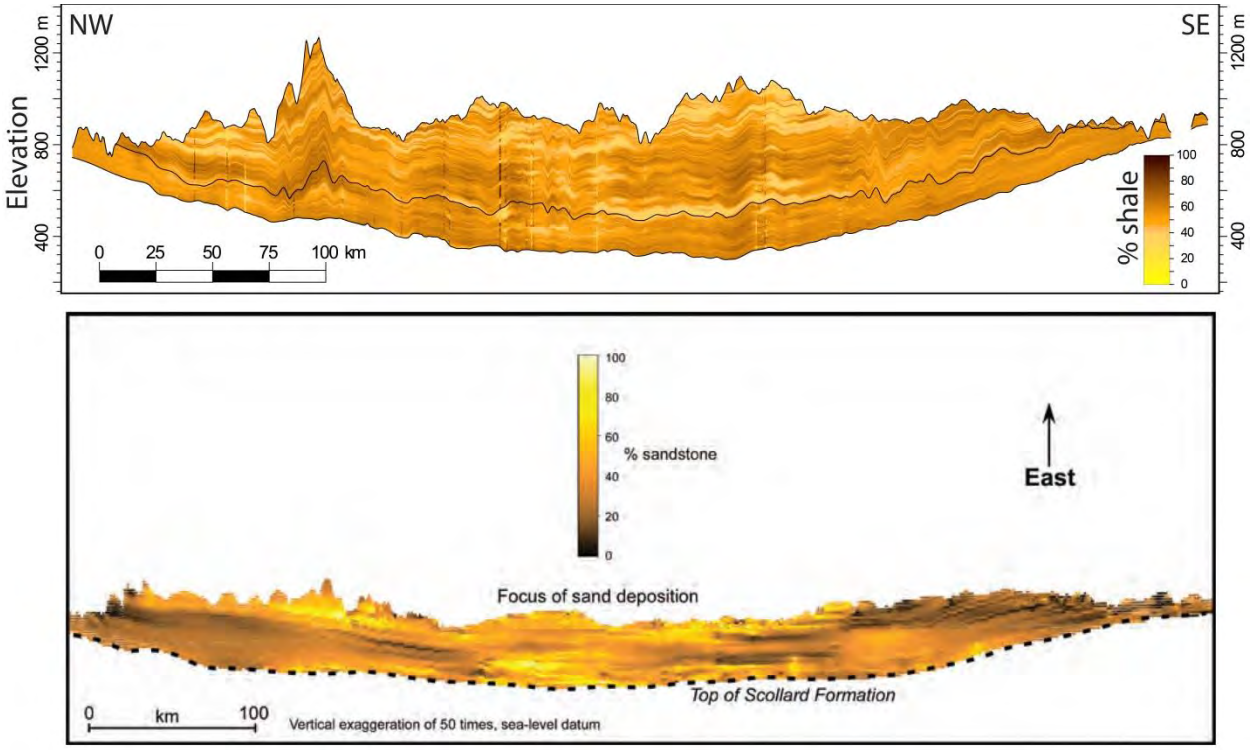

Figure 19, Comparison of the shale percentage model (upper) with the sandiness model of Lyster and Andriashek (2012) (lower). The black line across the cross-section in the upper image indicates the boundary between the Paskapoo Formation and the Scollard Formation. The cross-section location is shown by line 6 in Figure 1. Vertical exaggeration is 100 times (upper) and 50 times (lower).

This 3D property model provides insight into the vertical and lateral connectivity of sandstone units and the degree of confinement (or compartmentalization) of the surrounding mudstone. The 100 realizations help to overcome the shortcomings of the kriging algorithm, which tends to smooth out local details of the spatial variation in connectivity. Lyster and Andriashek (2012) demonstrated that the simulation results can be used to estimate the internal geometry of sand units and connectivity of the Paskapoo Formation. Zones having a high sandiness are likely to be more transmissive than surrounding sediments, and the spatial distribution pattern establishes a basis to define the internal architecture of individual formations. This 3D property model can be used to conceptualize the hydrostratigraphy assuming that the sandiness value, in terms of shale percentage inversely, is a proxy for permeability. Knowledge of the 3D sandstone unit geometry is useful for identifying localized aquifers and the extent of hydrogeological pathways. The 3D property model could help inform hydrostratigraphic conceptualization at a scale considerably finer than geological formations (Figure 20).

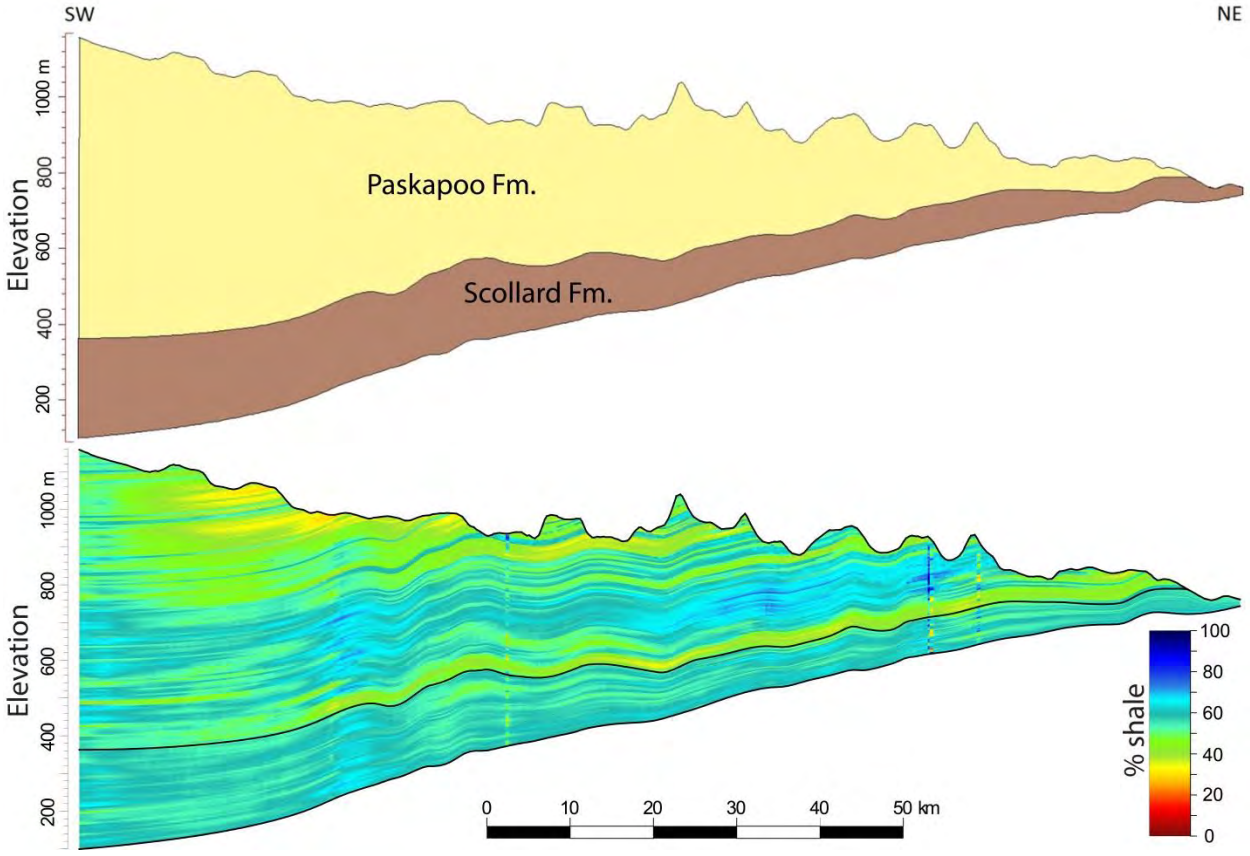

Figure 20. Comparison of cross-sections of geological formations and the kriged shale percentage model. The cross-section's location is shown by line 3 in Figure 1. Vertical exaggeration is 45 times.

9 References

Alberta Geological Survey (2015): Alberta table of formations; Alberta Energy Regulator / Alberta Geological Survey, URL <https://ags.aer.ca/activities/table-of-formation> [August 2018].

Alberta Geological Survey (2019): 3D provincial geological framework model of Alberta, version 2; Alberta Energy Regulator / Alberta Geological Survey, AER/AGS Model 2018-02.

Braman, D.R. and Sweet, A.R. (1990): Overview of Campanian to Paleocene stratigraphy, southern Alberta Foothills *in* D.R. Braman and A.R.Sweet (ed.), Field guide to uppermost Cretaceous Strata in southern Saskatchewan and Alberta, Canadian Society of Petroleum Geologists Annual Convention Fieldtrip Guide, p. 66-70.

Branscombe, P., MacCormack, K.E., Babakhani, M. (2018): 3D Provincial Geological Framework Model V.1 - Methodology; Alberta Energy Regulator, AER/AGS Open File Report 2017-09, 114p. URL <https://ags.aer.ca/document/OFR/OFR_2017_09.pdf> [August 2018].

Burns, E.R., Bentley, L.R., Hayashi, M., Grasby, S.E., Hamblin, A.P., Smith, D.G. and Wozniak, P.R.J. (2010): Hydrogeological implications of paleo-fluvial architecture for the Paskapoo Formation, SW Alberta, Canada: a stochastic analysis; Hydrogeology Journal, 18(6): p. 1375–1390.

Chen, Z., Grasby, S.E. and Wozniak, P.R.J. (2007): Paskapoo groundwater study part VI: Aquifer transmissivity estimation and a preliminary data analysis of the Paskapoo Formation, Alberta; Geological Survey of Canada, Open File 5444, 31 p.

Daly, C., Quental, S. and Novak, D. (2010): A faster, more accurate Gaussian simulation; GeoCanada Conference, Calgary, AB, Canada, p. 10-14.

Demchuk, T.D. and Hills, L.V. (1991): A re-examination of the Paskapoo Formation in the central Alberta Plains: the designation of three new members; Bulletin of Canadian Petroleum Geology, 39(3): p. 270–282.

Alberta Energy and Utilities Board (2006): Directive 043: well logging requirements — surface casing interval; Alberta Energy and Utilities Board, URL <https://www.aer.ca/documents/directives/Directive043.pdf> [August 2018].

Fogg, G.E. (1986): Groundwater flow and sand body interconnectedness in a thick multiple aquifer system; Water Resources Research, v. 22, p. 679–694.

Folk, R.L. (1968): Petrology of sedimentary rocks; Hemphill's Publishing Company, Austin, Texas, 170 p.

Grasby, S., Tan, W., Chen, Z. and Hamblin, A.P. (2007): Paskapoo groundwater study part I: Hydrogeological properties of the Paskapoo Formation determined from six continuous cores; Geological Survey of Canada, Open File 5392, 6 p.

Grasby, S.E., Chen, Z., Hamblin, A.P., Wozniak, P.R.J. and Sweet, A.R. (2008): Regional characterization of the Paskapoo bedrock aquifer system, southern Alberta; Canadian Journal of Earth Sciences, 45(12): p. 1501–1516.

Gibson, D.W. (1977): Upper Cretaceous and Tertiary coal-bearing strata in the Drumheller-Ardley region, Red Deer Valley, Alberta; Geological Survey of Canada, Paper 76–35, 41 p.

Hamblin, A.P. (2004): Paskapoo-Porcupine Hills formations in western Alberta: synthesis of regional geology and resource potential; Geological Survey of Canada, Open File 4679, 30 p.

Hughes, A.T., Smerdon, B.D. and Alessi, D.S. (2017): A summary of hydraulic conductivity values for the Paskapoo Formation in West-Central Alberta; Alberta Energy Regulator, AER/AGS Open File Report 2016-03, 25 p. URL <https://ags.aer.ca/publications/OFR_2016_03.html> [August 2018]

Jerzykiewicz, T. (1997): Stratigraphic framework of the uppermost Cretaceous to Paleocene strata of the Alberta Basin; Geological Survey of Canada, Bulletin 510, 121 p.

Johnson, N.M. and Dreiss, S.J. (1989): Hydrostratigraphic interpretation using indicator geostatistics; Water Resources Research, v. 25, no. 12, p. 2501–2510.

Lerbekmo, J.F, Demchuk, T.D., Evans, M.E. and Hoye, G.S. (1992): Magnetostratigraphy and biostratigraphy of the continental Paleocene of the Red Deer valley, Alberta, Canada; Bulletin of Canadian Petroleum Geology, v. 40, no. 1, p. 24–35.

Lerbekmo, J.F., Heaman, L.M., Baadsgaard, K., Muehlenbachs, K., Evans, M.E. and Sweet, A.R. (2008): Normal polarity magnetosubchrons in 24r and the age of the Paleocence-Eocene boundary; Canadian Journal of Earth Sciences, v. 45, no. 7, p. 781–793.

Lerbekmo, J.F. and Sweet, A.R. (2000): Magnetostratigraphy and biostratigraphy of the continental Paleocene in the Calgary area, southwestern Alberta; Bulletin of Canadian Petroleum Geology, v. 48, no. 4, p. 285–306.

Lerbekmo, J.F. and Sweet, A.R. (2008): Magnetobiostratigraphy of the continental Paleocene upper Coalspur and Paskapoo formations near Hinton, Alberta; Bulletin of Canadian Petroleum Geology, v. 56, no. 2, p. 118–146.

Lyster, S. and Andriashek, L.D. (2012): Geostatistical rendering of the architecture of hydrostratigraphic units within the Paskapoo Formation, central Alberta; Energy Resources Conservation Board, ERCB/AGS Bulletin 66, 103 p. URL <https://ags.aer.ca/publications/BUL_066.html> [August 2018].

Nurkowski, J.R. (1985): Coal quality and rank variation within Upper Cretaceous and Tertiary sediments, Alberta Plains region; Alberta Research Council, ARC/AGS Earth Sciences Report 1985-01, 39 p. URL <https://ags.aer.ca/publications/ESR_1985_01.html> [August 2018].

Petrel Robertson Consulting Ltd. (PRCL) (2014): Aquifers in shallow bedrock and surficial sediments (Final Report); Petroleum Technology Alliance of Canada, 32 p.

Parks, K. and Andriashek, L. (2009): Preliminary investigation of potential, natural hydraulic pathways between the Scollard and Paskapoo formations in Alberta: implications for coalbed methane production; Energy Resources Conservation Board, ERCB/AGS Open File Report 2009-16, 66 p. URL <https://ags.aer.ca/publications/OFR_2009_16.html> [August 2018].

Prior, G.J., Hathway, B., Glombick, P.M., Pana, D.I., Banks, C.J., Hay, D.C., Schneider, C.L., Grobe, M., Elgr, R. and Weiss, J.A. (2013): Bedrock geology of Alberta; Alberta Energy Regulator, AER/AGS Map 600. URL <https://ags.aer.ca/publications/MAP_600.html> [August 2018].

Pyrcz, M.J. and Deutsch, C.V. (2014): Geostatistical reservoir modeling, 2nd ed.; Oxford University Press, 433 p.

Quartero, E.M., Leier, A.L., Bentley, L.R. and Glombick, P. (2015): Basin-scale stratigraphic architecture and potential Paleocene distributive fluvial systems of the Cordilleran Foreland Basin, Alberta, Canada; Sedimentary Geology, 316: p. 26–38.

Shier, D.E. (2004): Well log normalization: methods and guidelines; Petrophysics, 45.3, p. 268–280.

Slattery, S.R., Barker, A.A., Andriashek, L.D., Jean, G., Stewart, S.A., Moktan, H. and Lemay, T.G. (2011): Bedrock topography and sediment thickness mapping in the Edmonton–Calgary Corridor, central Alberta: an overview of protocols and methodologies; Energy Resources Conservation Board, ERCB/AGS Open File Report 2010-12, 16 p. URL <https://ags.aer.ca/publications/OFR_2010_12.html> [August 2018].

Williams, M.Y. and W.S. Dyer (1930): Geology of southern Alberta and southwestern Saskatchewan; Geological Survey Memoir 163, 160 p.

Appendix – Variograms and variogram parameters

Figure 21. Variogram model for the shale percentage variable in the zone for the Paskapoo and Porcupine Hills formations. Top right: vertical direction; bottom left: major direction; bottom right: minor direction. Black squares: experimental variograms; blue lines: modelled variogram functions; red/green/purple/cyan squares: individual variogram function ranges and sills; grey line: least squares regression line; grey bars: number of variogram pairs at each lag.

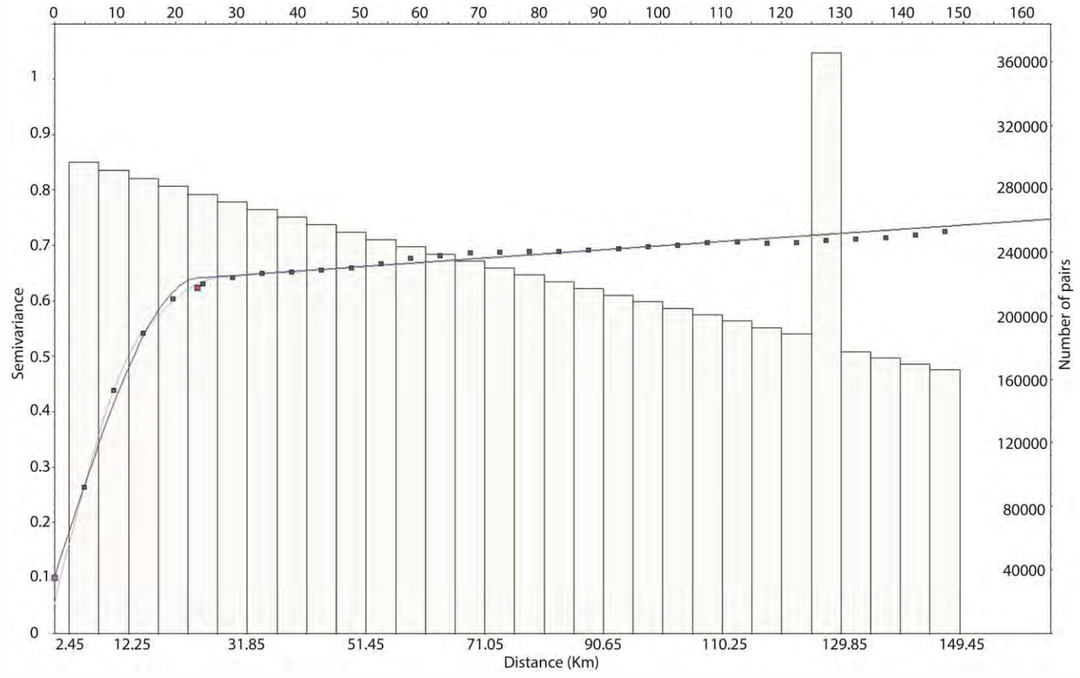

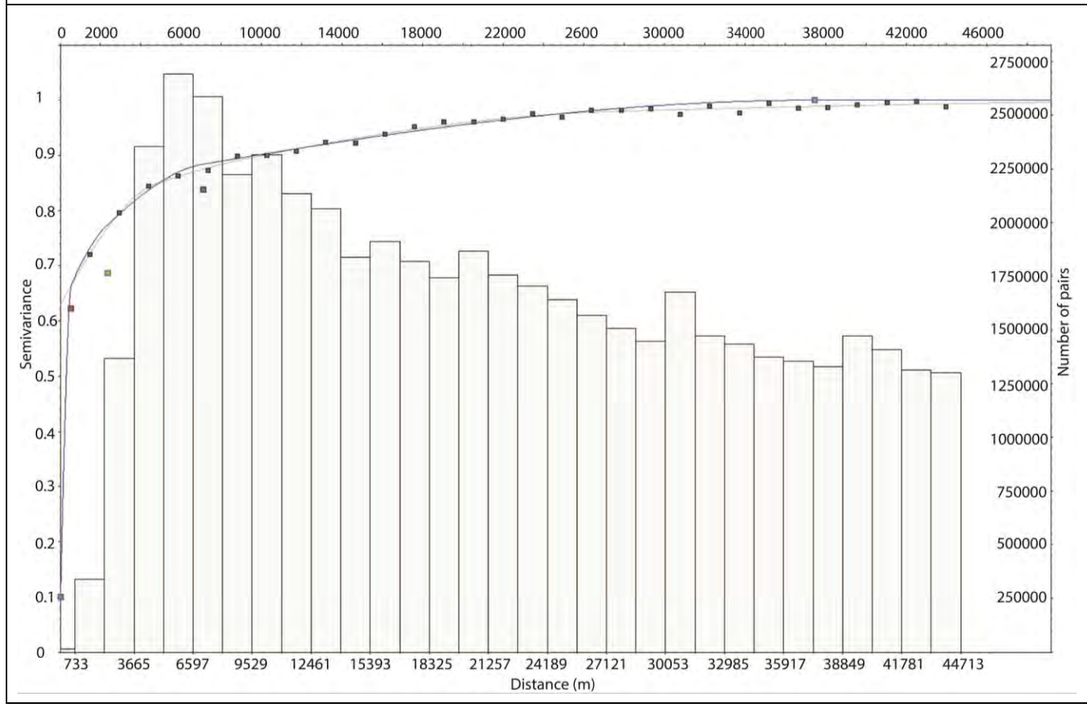

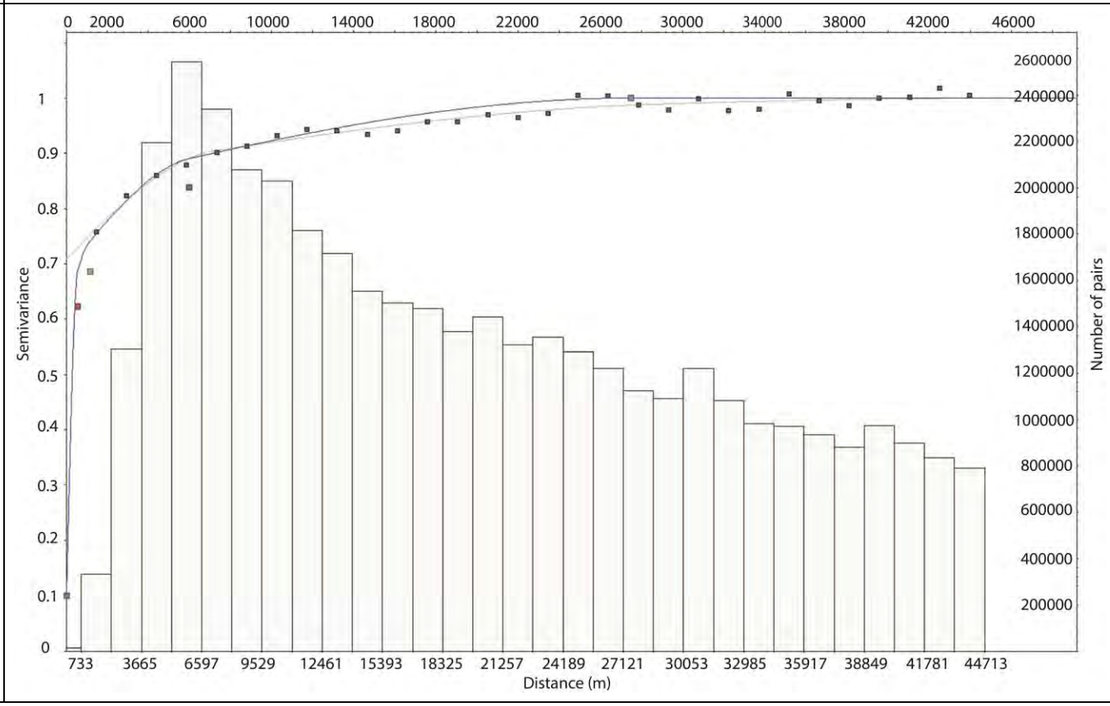

Figure 22. Variogram model for the shale percentage variable in the zone for the Scollard and Willow Creek formations. Top right: vertical direction; bottom left: major direction; bottom right: minor direction. Black squares: experimental variograms; blue lines: modelled variogram functions; red/green/purple/cyan squares: individual variogram function ranges and sills; grey line: least squares regression line; grey bars: number of variogram pairs at each lag.

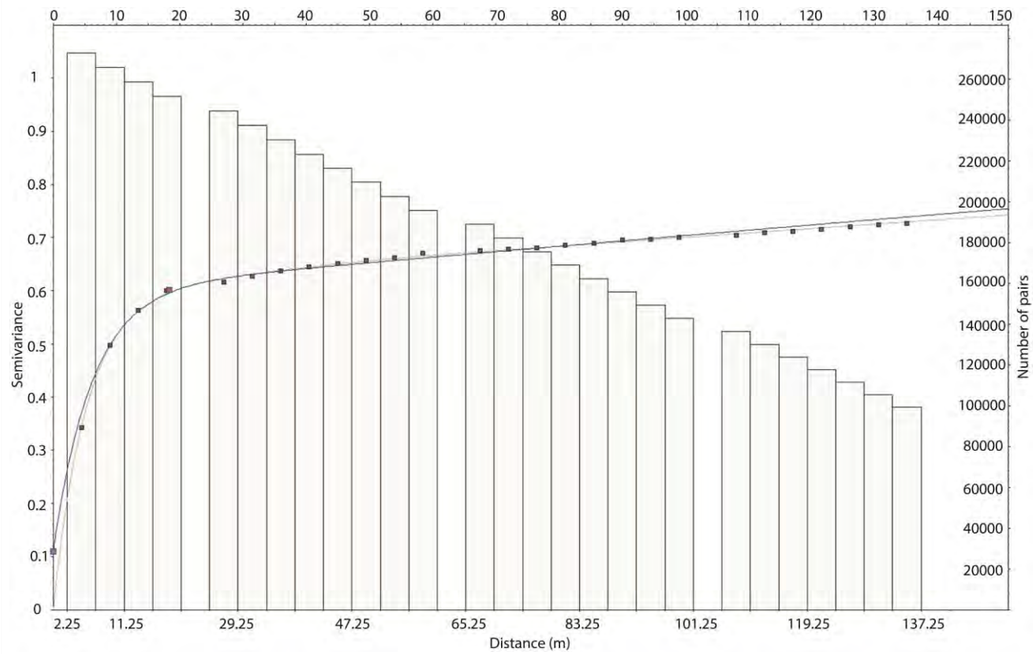

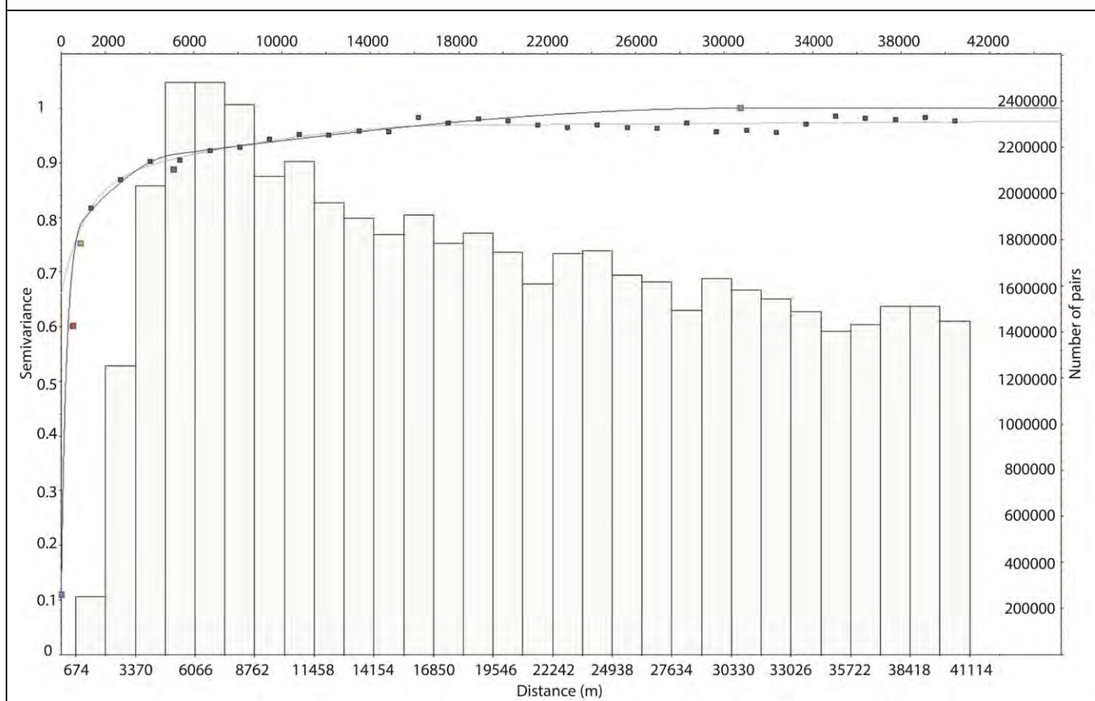

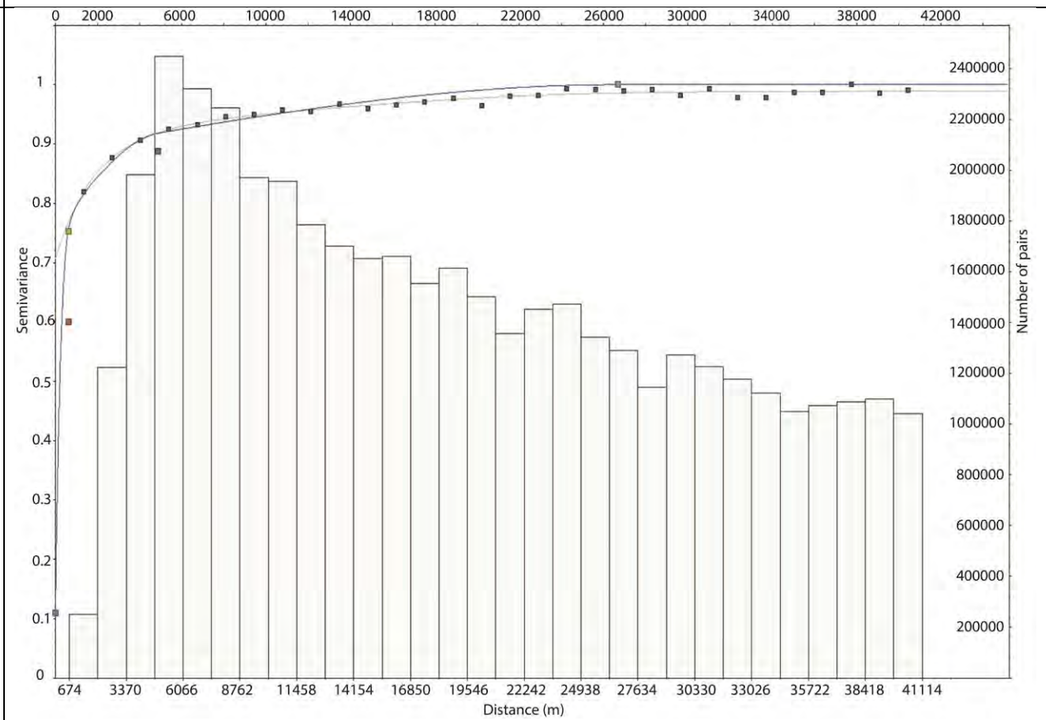

Figure 23. Variogram model for the density porosity variable in the zone for the Paskapoo and Porcupine Hills formations. Top right: vertical direction; bottom left: major direction; bottom right: minor direction. Black squares: experimental variograms; blue lines: modelled variogram functions; red/green/purple/cyan squares: individual variogram function ranges and sills; grey line: least squares regression line; grey bars: number of variogram pairs at each lag.

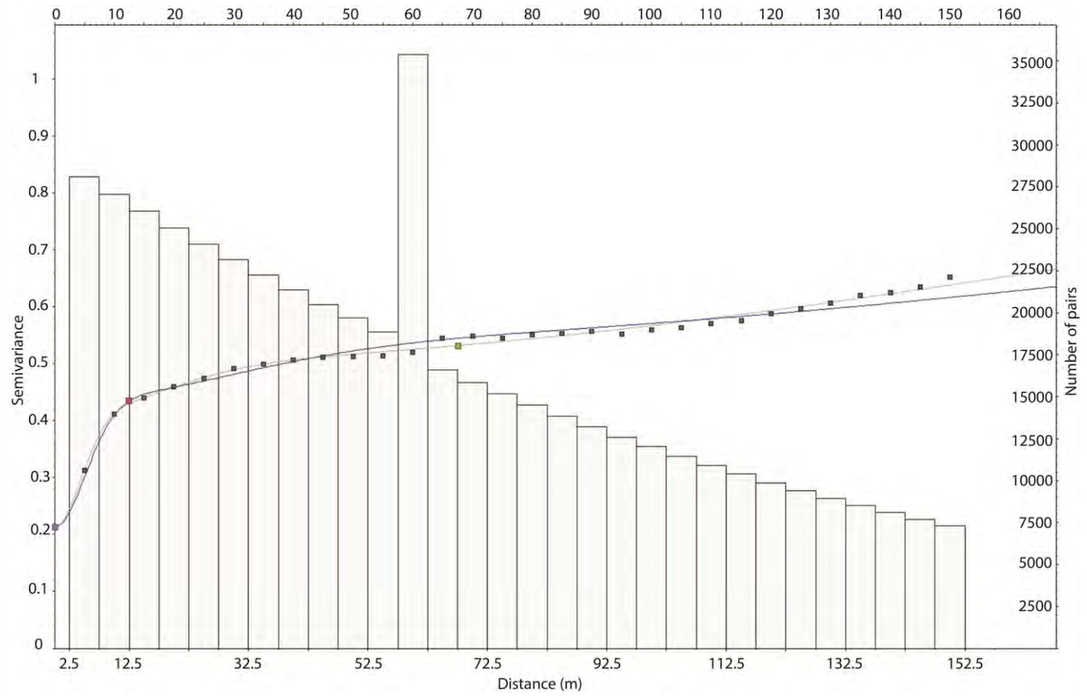

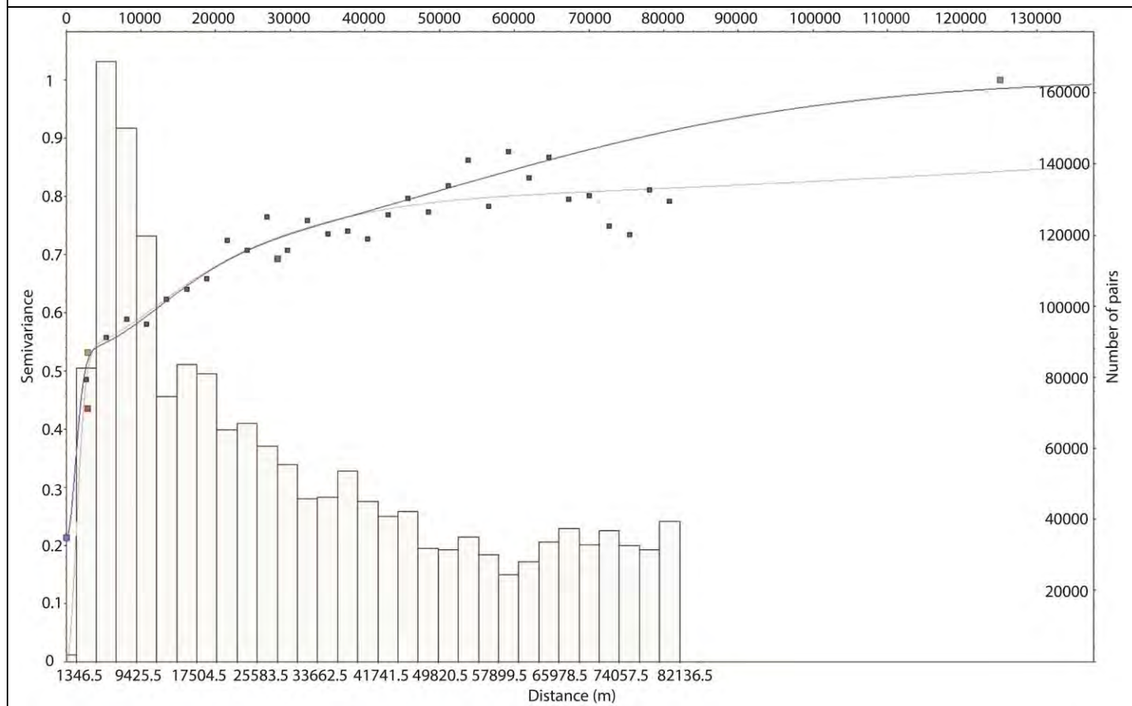

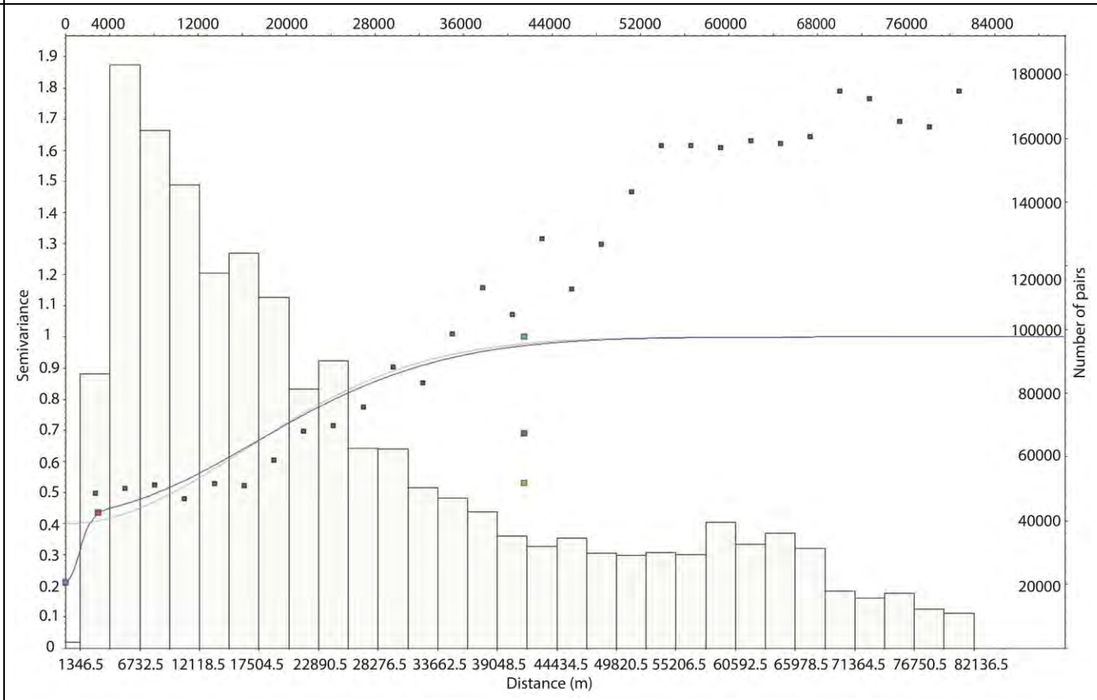

Figure 24. Variogram model for the density porosity variable in the zone for the Scollard and Willow Creek formations. Top right: vertical direction; bottom left: major direction; bottom right: minor direction. Black squares: experimental variograms; blue lines: modelled variogram functions; red/green/purple/cyan squares: individual variogram function ranges and sills; grey line: least squares regression line; grey bars: number of variogram pairs at each lag.

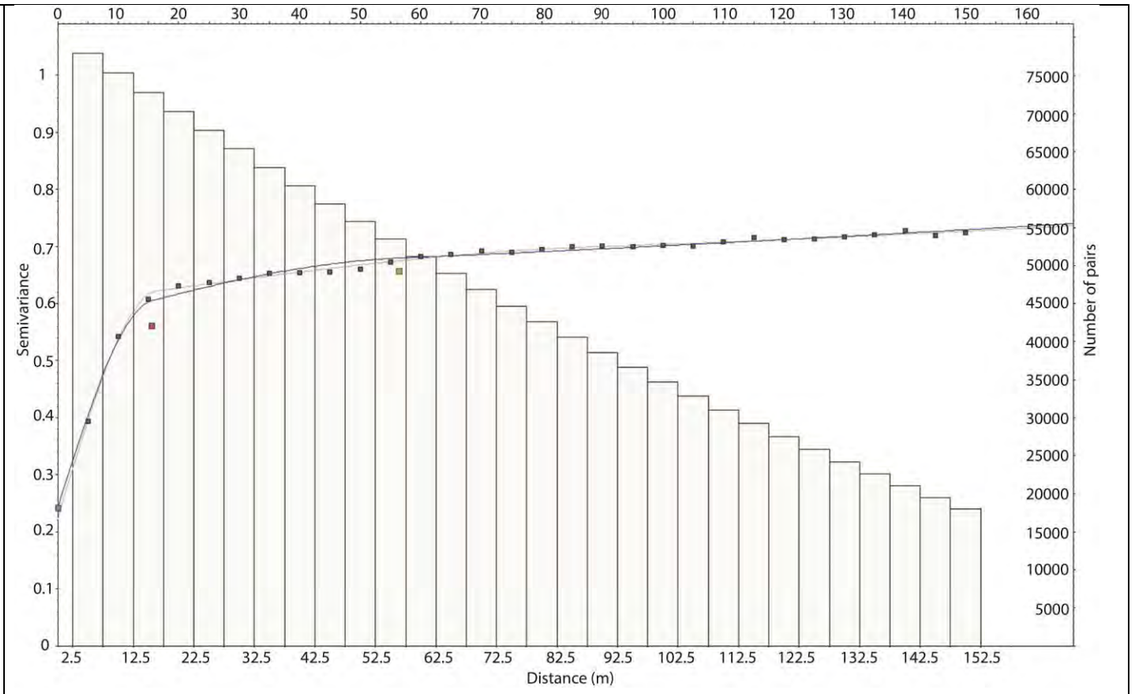

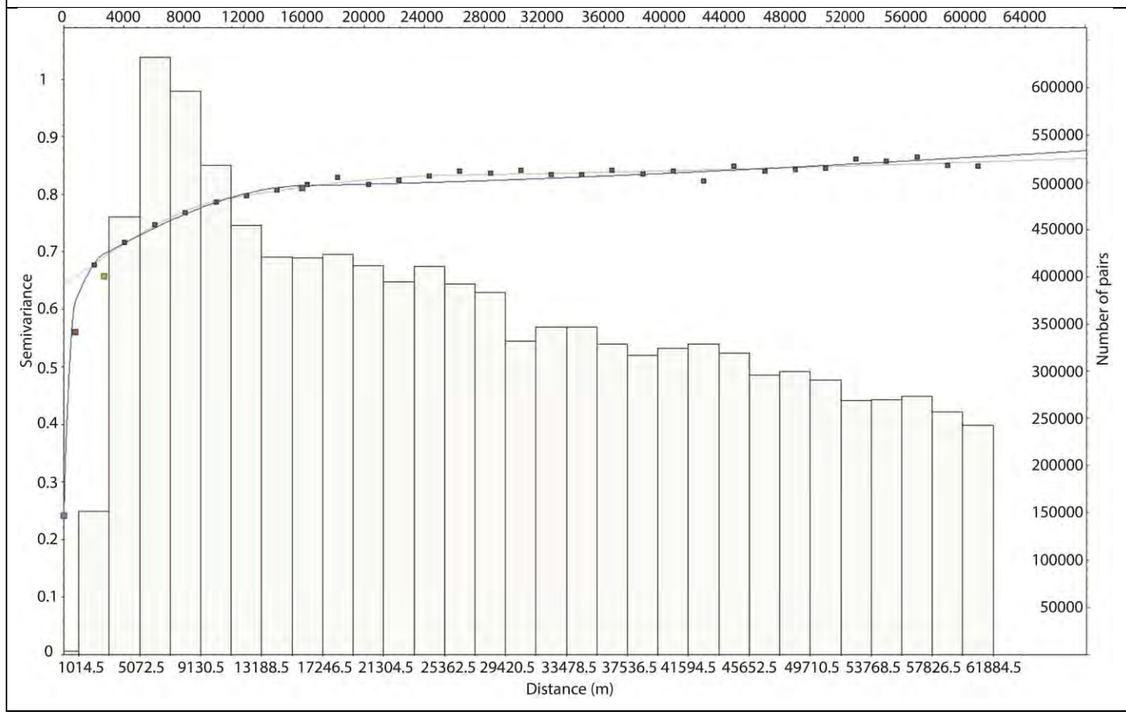

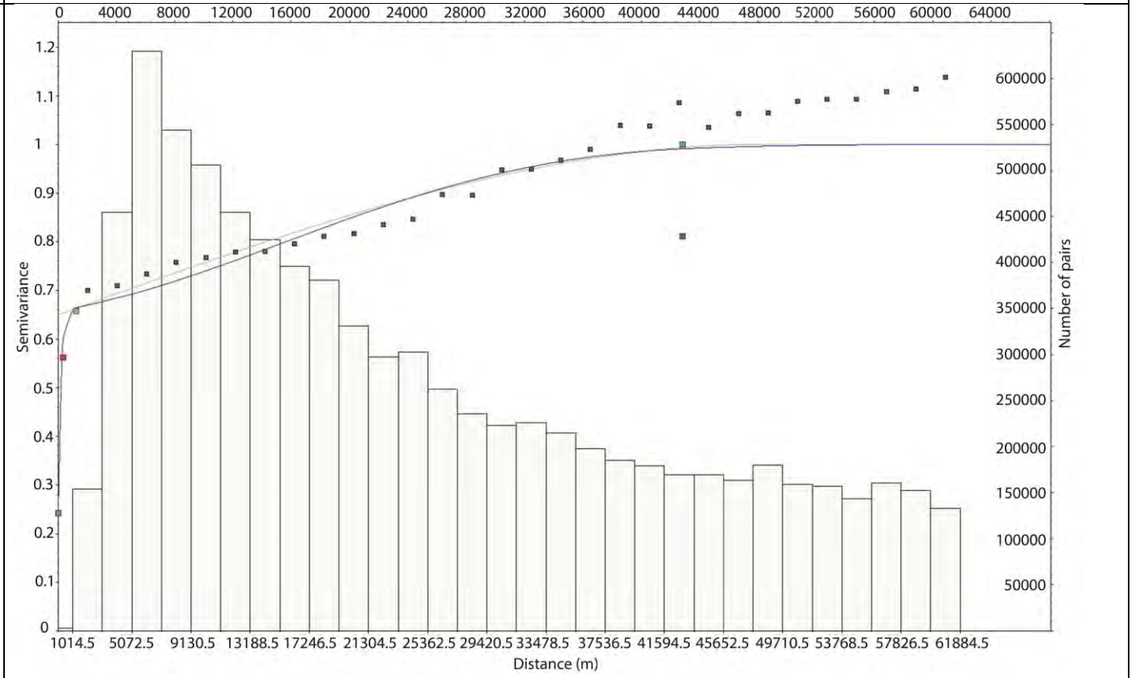

Figure 25. Variogram model for the shale percentage variable derived from water wells for all zones. Top right: vertical direction; bottom left: major direction; bottom right: minor direction. Black squares: experimental variograms; blue lines: modelled variogram functions; red/green/purple squares: individual variogram function ranges and sills; grey line: least squares regression line; grey bars: number of variogram pairs at each lag.

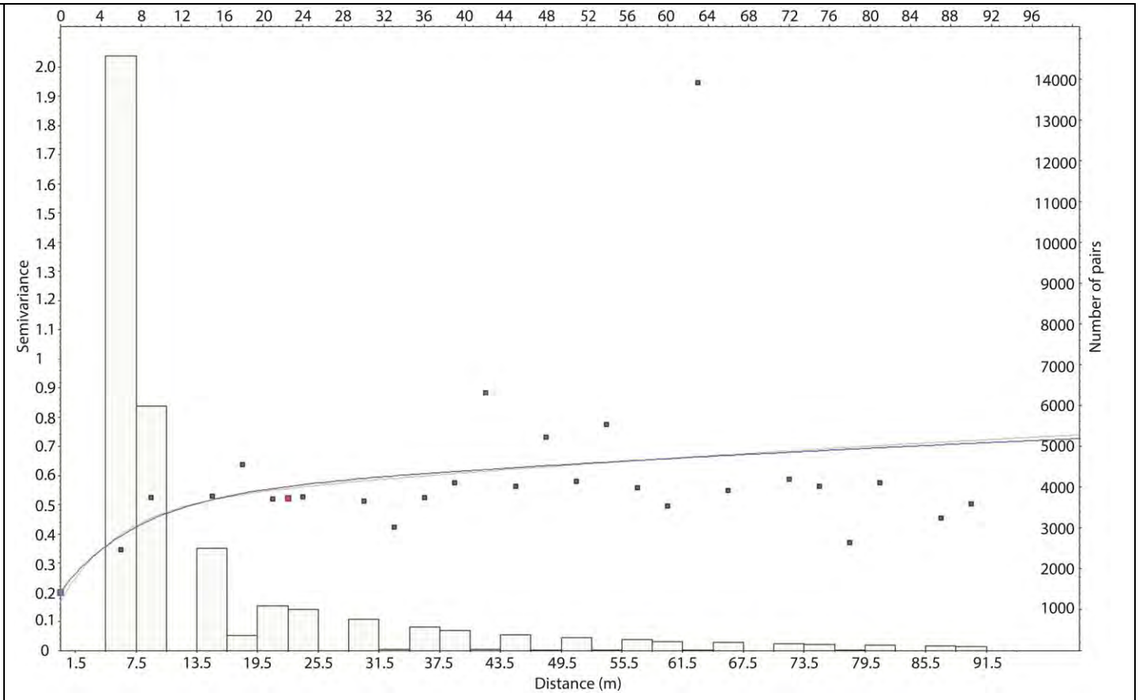

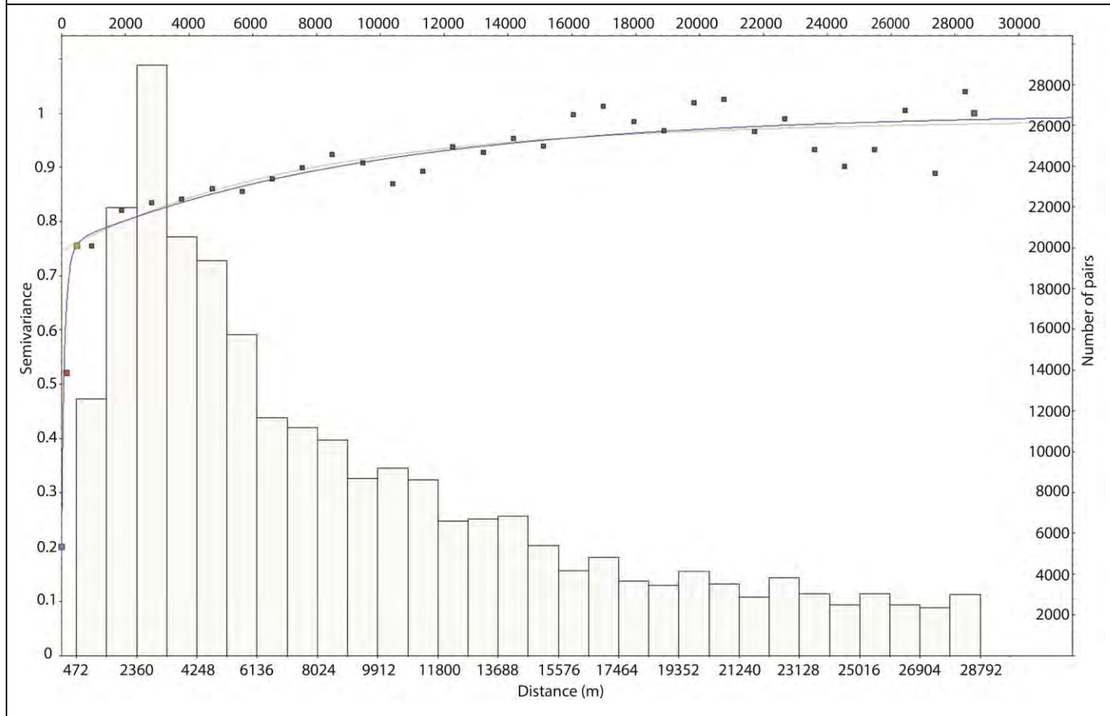

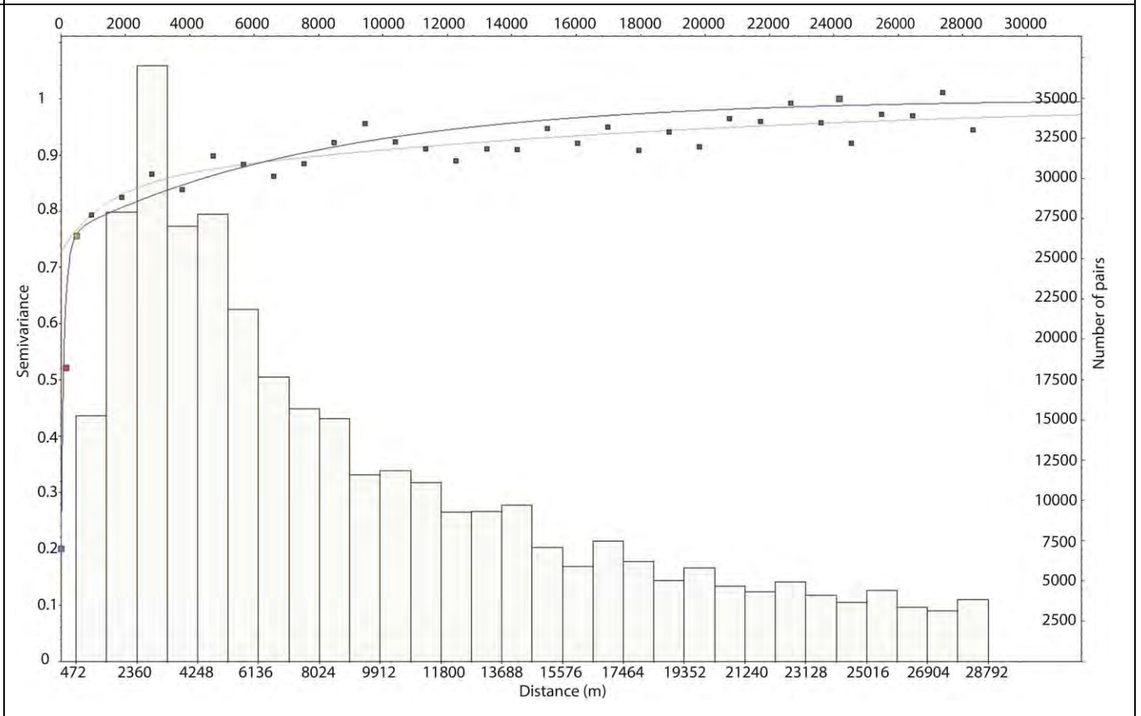

Table 1. Variogram parameters for the shale percentage variable in the 3D property model.

Zone	Major horizontal direction	Structure	Model function	Sill	Vertical range	Major horizontal range	Minor horizontal range
Paskapoo-Porcupine Hills	135 degrees	0	Nugget	0.1000			
		1	Spherical	0.5228	23.661	550.774	1021.888
		2	Spherical	0.0635	725.156	1185.739	2363.523
		3	Spherical	0.1522	735.000	5993.994	6135.328
		4	Spherical	0.1615	735.000	27481.952	28942.405
Scollard	135 degrees	0	Nugget	0.1100			
		1	Spherical	0.4909	18.332	548.327	624.092
		2	Spherical	0.1514	559.584	894.882	624.092
		3	Spherical	0.1354	559.584	5101.725	4872.738
		4	Spherical	0.1123	620.100	30740.259	26673.51

Table 2. Variogram parameters for the density porosity variable in the 3D property model.

Zone	Major horizontal direction	Structure	Model function	Sill	Vertical range	Major horizontal range	Minor horizontal range
Paskapoo-Porcupine Hills	135 degrees	0	Nugget	0.2127			
		1	Gaussian	0.2221	12.435	2928.966	2951.213
		2	Gaussian	0.0958	67.649	2928.966	41454.371
		3	Gaussian	0.161	578.426	28345.541	41454.371
		4	Gaussian	0.3084	578.426	125013.682	41454.371
Scollard	135 degrees	0	Nugget	0.2411			
		1	Spherical	0.3196	15.593	776.6	347.296
		2	Spherical	0.0963	56.383	2677.597	1248.277
		3	Spherical	0.1531	664.816	15910.529	42846.882
		4	Gaussian	0.1899	750.000	181732.92	42846.881

Table 3. Variogram parameters for the water well derived shale percentage variable in the 3D property model.

Zone	Major horizontal direction	Structure	Model function	Sill	Vertical range	Major horizontal range	Minor horizontal range
All zones	45 degrees	0	Nugget	0.200			
		1	Exponential	0.321	22.491	166.300	165.627
		2	Exponential	0.2341	430.859	500.001	500.262
		3	Exponential	0.2449	683.663	28591.505	24162.391